5-2021

Simulation of Transient Conditions in Vehicle-to-Grid Systems Fed from Plug-in Electric Vehicles

Olapade Oludolapo Olagbemi
Western Michigan University, padeOlagbemi@outlook.com

Simulation of Transient Conditions in Vehicle-to-Grid Systems Fed from Plug-in Electric Vehicles

by

Olapade Oludolapo Olagbemi

A thesis submitted to the Graduate College
in partial fulfillment of the requirements for
the degree of Master of Science in Engineering
Electrical and Computer Engineering
Western Michigan University
May 2021

Thesis Committee:

Pablo Gómez, Ph.D., Chair
Richard T. Meyer, Ph.D., Co-Chair
Damon A. Miller, Ph.D.

Simulation of Transient Conditions in Vehicle-to-Grid Systems
Fed from Plug-in Electric Vehicles

Olapade Oludolapo Olagbemi, M.S.E.

Western Michigan University, 2021

The increasing adoption of plug-in electric vehicles for commercial and consumer needs, coupled with government targets and incentives for use of renewable energy sources and reduction of greenhouse gases [1, pp. 44-45], has led to their consideration as power sources. Such vehicle-to-grid (V2G) systems seek to take advantage of the aggregate energy available within fleets of electric vehicles connected to power grids through bi-directional charging stations, by using them as distributed power sources for load leveling and peak shaving on the power grids [2]. Unfortunately, V2G systems can introduce power quality issues, such as harmonics, with associated transients that pose a threat to the reliability and stability of traditional power grids [3].

This study examines the transient behavior of a test V2G system under varying vehicle and grid load conditions. The operation of a controlled bi-directional converter, in transient states related to voltage and load variance, is demonstrated using Simulink®. Estimation of network model component parameters is addressed. The resulting model is able to simulate the relationship between network transients and variations in grid loads under different operational scenarios, for potential application in the design and testing of V2G control and protection schemes.

ACKNOWLEDGEMENTS

This work would not have been possible without the kind support of several persons, some of whom might not be mentioned here. Their contributions in ways big or small made it possible to complete this work. I would, however, like to mention a few of them.

My sincere thanks go to my supervisor, Dr. Pablo Gómez, for the opportunity to work on this thesis, and for his guidance and support throughout the study. I wish to thank the rest of my thesis committee – Dr. Rick Meyer and Dr. Damon Miller – for their support and time, especially during the busy weeks near the end of the semester. Together, they enhanced the quality of the learning experience I had while completing this study. I would also like to thank the Power Equipment Simulation and Design Laboratory at Western Michigan University, Kalamazoo, for the use of the server and software on which all the simulations were run.

Finally, I wish to acknowledge the support of my family – for their understanding and patience while I worked through the project.

Olapade Oludolapo Olagbemi

TABLE OF CONTENTS

Table of Contents – Continued

CHAPTER

LIST OF TABLES

LIST OF FIGURES

List of Figures – Continued

LIST OF ABBREVIATIONS

AC	Alternating Current
BEV	Battery Electric Vehicle
BMS	Battery Management System
DC	Direct Current
ESS	Energy Storage System
EV	Electric Vehicle
HEV	Hybrid Electric Vehicle
ICE	Internal Combustion Engine
PEV	Plug-in Electric Vehicles
PHEV	Plug-in Hybrid Electric Vehicles
PWM	Pulse Width Modulation
RMS	Root Mean Square
rpm	Revolutions per Minute
SoC	State of Charge
THD	Total Harmonic Distortion
V2G	Vehicle-to-Grid

1. INTRODUCTION

Vehicle-to-grid (V2G) systems involve bi-directional power transfers between battery energy systems in plug-in electric vehicles (PEV) and the connected power grid. Apart from the uncertainties regarding the availability – and hence capacity – of such distributed vehicular-based power systems, injecting power from inverter-based sources requires a grid capable of tolerating harmonics as well as the transients associated with the V2G load changes.

1.1. Problem Statement

Electric vehicle (EV) charging systems incorporate switched inverters and rectifiers, which are sources of high-frequency harmonics. Connecting such sources of harmonics to the power grid introduces a higher risk of early equipment failure, and potentially affects grid power quality and stability. Also, since the primary function of vehicles is transportation, the availability of any particular vehicle on the grid is uncertain. While work and operational cycles may be used to predict vehicle availability for aggregate planning purposes, the grid operator has no control over actual connection times and durations. As demand on the grid and connected battery capacity vary, there is a need for the V2G system to respond to load and source variations in a timely and optimal manner, and with minimal transient disturbance, for power systems safety and grid operational efficiency.

1.2. Thesis Objectives

The primary objective is to create a model of a vehicle-to-grid (V2G) system capable of supporting the study of transient voltages and currents, as well as the testing of control algorithms for practical V2G systems. Additional objectives include the design and implementation of model building blocks, representative of the operations of the V2G system components: power grid, bi-directional AC-DC converter, vehicle fleet and associated battery systems.

This study involves the simulation of a V2G system using Simulink®, a software simulation environment for dynamic systems. The component building blocks implemented will be adaptable for use in future V2G models.

1.3. Thesis Contributions

Changes in V2G load or operational mode could trigger different transient behaviors at different points in the system. In view of the consideration that such transients are potentially harmful to traditional power grid equipment [3], a question arises as to the types and magnitudes of transients generated by the operation of the V2G hardware, and the degree to which they are significant in affecting existing grid power quality, and consequently, reliability.

Both steady-state and transient behaviors of V2G systems have received attention in prior research. This thesis seeks to examine the transients created by the different modes of change in the V2G system. The study focuses on the transient behavior of V2G systems, considering its importance for the accurate prediction of oscillatory behavior that could result in power quality issues, as well as potential failure or damage of connected equipment.

1.4. Thesis Outline

Chapter 1 introduces the concept of V2G systems and describes its relevance and associated problems. The second chapter is a literature review of V2G in terms of state-of-the-art and relationship to this study. Different schemes for operation of V2G are discussed as well as merits and challenges.

Chapter 3 includes a detailed design of the V2G system, followed by its modeling. System modules are described along with signal and control interfaces. The implementation in the simulation environment is presented. Chapter 4 presents the test results while Chapter 5 summarizes the findings and conclusions, and presents recommendations for future research.

2. LITERATURE REVIEW

Electric vehicles in various forms have become increasingly common in daily use. The increasing adoption of plug-in electric vehicles for commercial and consumer needs, coupled with government targets for use of renewable energy sources [1, pp. 44-45], has led to consideration of such vehicles as temporary distributed power sources. The concept of vehicle-to-grid (V2G) systems, as they are known, recognizes the opportunities for load leveling and peak shaving that exist within fleets of electric vehicles connected to a charging grid. Such vehicles can inject stored energy back into the power grid when desired, provided the appropriate equipment and management system are implemented. In this chapter, existing research in the area of V2G systems is examined. A few approaches for implementation and control of V2G components are discussed.

2.1. Background

A V2G system involves coordination of multiple systems to achieve network power flow objectives. On the grid, it is desirable to have as flat a load profile as possible that is free of harmful harmonics. Vehicle operators require vehicle battery levels – monitored through battery management systems – to be within limits required for acceptable operation at the end of the charge period. V2G enables storing of excess grid energy in vehicle batteries during periods of low demand, and its release back to the grid during periods of higher demand [4]. In practice, harmonics are always present since the power converters in vehicle charging systems incorporate power electronic switching devices.

2.2. Plug-In Electric Vehicles in Context

To provide some context for this study, two broad categories of electric vehicles (EVs) are considered: hybrid electric vehicles (HEVs) and plug-in electric vehicles (PEVs). The HEV drivetrain incorporates an internal combustion engine (ICE) coupled with an electric motor. The electric motor is powered from a separate on-board energy storage system (ESS), which includes a battery pack and an energy management system. A generator driven by the ICE charges the battery pack in a HEV; no plug-in feature is included. A popular example is the 2010 Toyota Prius [5, pp. 3-4] and [6, pp. 5-1].

Battery electric vehicles (BEVs) rely solely on their on-board batteries for power, as shown in Figure 1. Consequently, their battery packs have much higher storage capacities than HEV battery packs and need to be recharged from external power sources. Within the categories of electric vehicles currently in use, BEVs have among the highest installed capacities of on-board energy storage systems [1]. The Nissan Leaf and Tesla models are well known examples of BEVs.

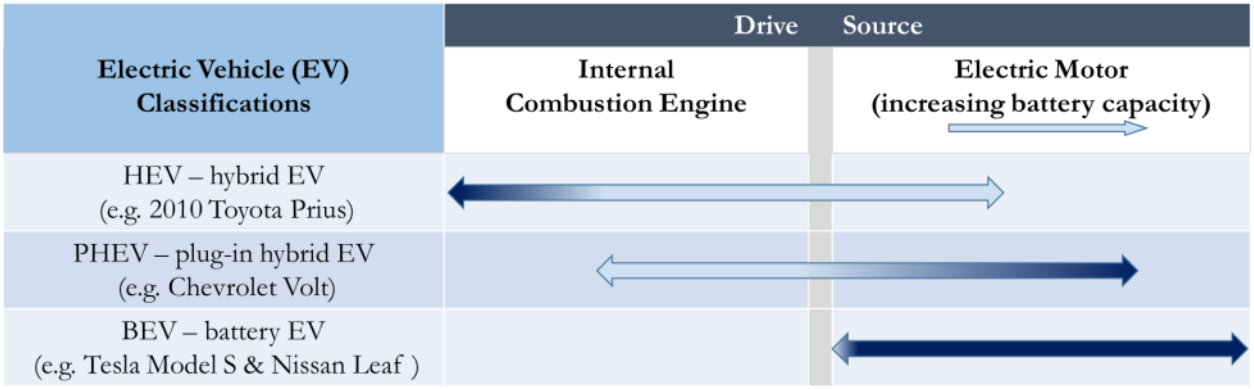

Figure 1. Classifications of electric vehicles with respect to drive source and battery capacity

Plug-in hybrid electric vehicles (PHEVs) may be regarded as BEVs that also have internal combustion engines. They rely mainly on the ESS battery and use the internal combustion as a back-up to extend travel range between recharges. Their battery pack capacities lie somewhere between those of the BEVs and HEVs. The Chevrolet Volt [7] is an example of a PHEV. The blend of electric versus internal combustion capacities varies among manufacturers. Subsequent usage of the term 'PEV' in this study refers to both BEVs and PHEVs.

2.3. Discussion and Theory

The block diagram in Figure 2 shows the modules of a typical vehicle-to-grid system. In order to adjust for changing load requirements, the controller – which could be a network of communicating systems – monitors the load on the power grid and the vehicle battery states provided via signals from the battery management systems in the fleet. A control algorithm utilizes these signals to determine the mode of operation of the bi-directional AC-DC converter as well as the intensity of its response, in order to maintain network parameters at their target values. The response is limited by the energy capacity available in the fleet.

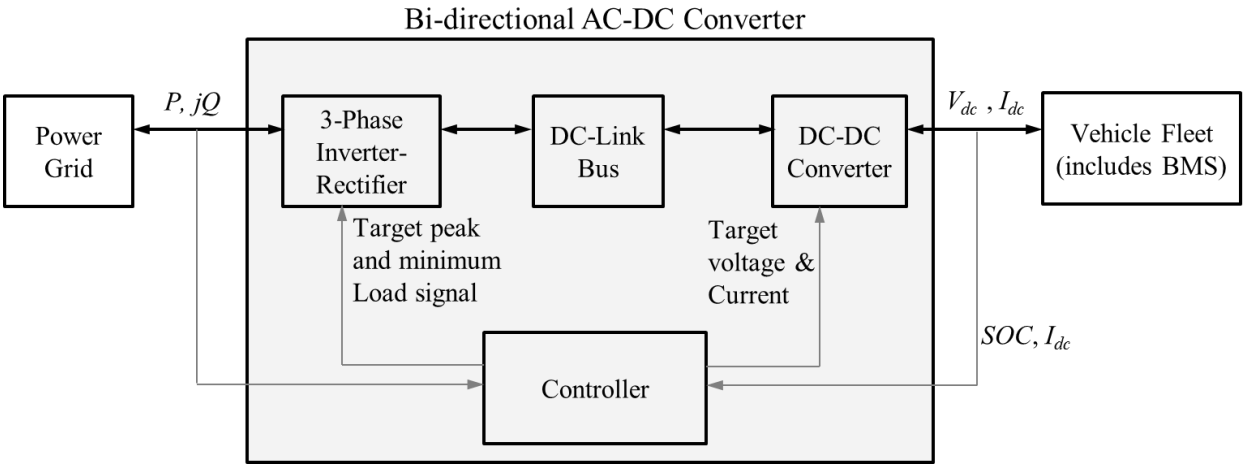

Figure 2. Block diagram of vehicle-to-grid system modules

2.3.1. Power Grid Characteristics

In the United States, electric power is distributed at voltages between 15 kV and 34.5 kV [8]. Higher voltage levels are used, as the power requirement increases, in order to minimize system losses from higher current levels. According to [9], voltages from 2.5 kV to 34.5 kV are regulated within ±10%. The increased adoption of distributed energy sources, coupled with the inherent variations in their availability and capacity, has increased the potential for power grid voltage fluctuations, making it increasingly necessary to look beyond traditional methods of voltage regulation, i.e. voltage taps and reactive power control [10]. Thus, [10] propose several technologies, including distributed voltage control via a distribution point, using voltage control devices and reactive power compensation from connected inverter sources. They also recommend a coordinated voltage control strategy – a volt-var optimization across all control devices in the distribution network.

The foregoing demonstrates the need for a V2G source to provide some voltage control at its point of connection to the grid, and contrasts that with the need to coordinate this operation with overall optimization of grid voltage regulation.

2.3.2. Vehicle Fleet Characteristics

The availability of PEVs was initially thought to be too low to justify their consideration as meaningful sources for the grid. It is worth noting that the grid operator has no control over actual vehicle connection schedules; however, many vehicles were found to be in use for an average of about one hour per day [4]. According to [11] and [12], studies have shown that a

typical personal vehicle is parked on average up to 90% of the day. During these times, energy stored in vehicle battery systems could be available to meet utility demand during peak periods, with the batteries subsequently recharged during off-peak hours.

Kempton and Tomić [2] developed equations to calculate grid power capacity from various electric vehicle types, and the cost versus revenue of each type with respect to grid scenarios such as peak power and regulation. These could prove useful in modeling of optimal power flows from different categories of PEVs. However, in considering the available power from a specific vehicle, their study highlights several relevant parameters, including vehicle driving efficiency (which relates miles driven to energy used) and conversion efficiency of the vehicle AC-DC converter. The vehicle driving efficiency affects the state of charge after a trip, while the conversion efficiency limits the power that may be extracted, taking losses into account. Both of these can be monitored indirectly via the state of charge (SoC).

2.3.3. Vehicle ESS and BMS

The plug-in electric vehicle energy storage system (ESS), a critical component for its operation, includes the battery management system (BMS), the thermal management system and the battery pack. Modern ESS battery packs are constructed using nickel-metal-hydride (NiMH) [5, p. 6], or a variety of lithium-based compounds, such as lithium-ion (Li-ion), lithium-polymer [1], lithium ferro phosphate (LiFePo4) and lithium titanate (LTO) [13]. EV manufacturer design voltages for the ESS range from 200 V to 800 V [14]. The Prius has a maximum DC-DC converter voltage of 650 V and a battery nominal voltage of 201.6 V [5]. The Tesla, on the other hand, uses a 350 V battery rated 400 V (max) [15].

The BMS forms the primary interface between vehicles and the grid. It monitors the battery charge state, current and temperature, and controls the charging or discharging current to ensure that battery parameters, such as voltage, temperature and SoC remain within limits that maximize the battery operating life. The state-of-charge is a critical measurement for the operation of a V2G system. Different storage systems have different minimum safe SoCs. Consequently, there needs to be some form of communication between various modules to allow for the monitoring and control functions of the battery management system [1]. In [16], an approach for estimating the SoC using an equivalent circuit model of the ESS battery is described. However, the circuit parameters of the charging systems are not always readily available, making it difficult to accurately model them.

To overcome the unavailability of equivalent circuit parameters for proprietary equipment, [3] proposed a method of estimation using voltage and current measurements along with frequency-domain harmonic analytical modeling. This is better suited to scenarios where it is possible to take measurements over a range of operating conditions. Simpler approaches use known characteristics of the battery type and, where required, scale up the parameter values in line with the capacity required. In [16], this approach was found to result in discrepancies of 1.6% to 5.3% between measured and calculated parameter values.

Huria et al. [17] proposed a model based on one voltage source in series with a resistor and a parallel resistor-capacitor (RC) combination. In order to account for temperature effects, multiple RC bridges were considered. However, a single RC pair was found sufficient to model the non-linear relationship between battery terminal voltage and discharge level within 2% accuracy. In the equivalent circuit shown in Figure 3, R_{int} is the battery internal resistance and is a function of the SoC, as are R_{bat} and C_{bat}, which are required to account for the temperature-

dependent discharge dynamics of the battery. The terminal voltage, V_{Th}, is the Thévenin equivalent presented to the rest of the network and is also a function of SoC.

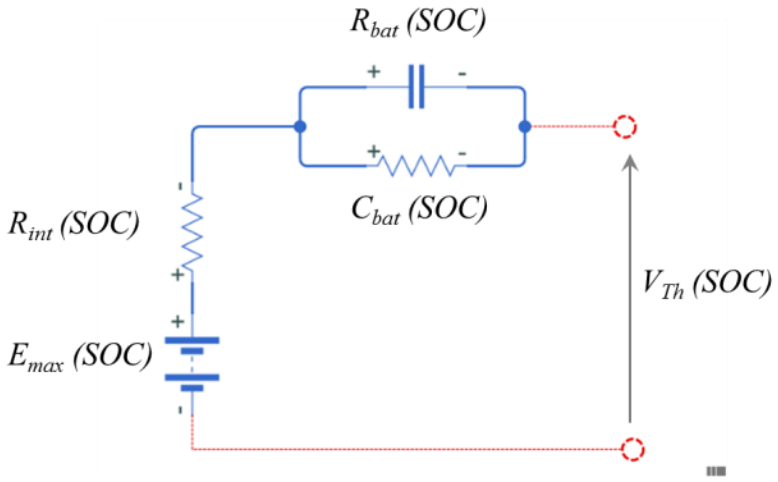

Figure 3. Equivalent circuit diagram of a rechargeable Li-ion battery

The state of charge (SoC) may be expressed as:

$$SoC = 1 - \frac{Q_C}{Q_{max}} \quad , \tag{2-1}$$

where Q_C is the net charge flow out of the battery and Q_{max} is the maximum battery capacity, measured in amp-hours [17].

2.3.4. Charging Methods and Devices

The vehicle battery management system and charging equipment determine the mode of operation (charging versus grid injection) and the rate of power flow. Signals from the grid convey requests for power through the charging equipment (the connection point) to the BMS. The BMS keeps track of the battery state of charge and controls the maximum power level of the inverter. Although OEM specifications for charging equipment vary among manufacturers, the

SAE J1772 standard specifies the requirements for performance as well as physical and electrical attributes [1]. At present, charging devices for PEVs are compatible with standard 115 V residential outlets. However, for V2G systems, higher capacity chargers are required, which require 240 V connections similar to high-current appliances found in most homes, and are available in both private and public facility connections. Power levels and charging modes are described in [1] and summarized in Table 1.

Table 1. Vehicle charging modes and power levels (extracted from [1])

PEV Charging Level	**Operating Voltage**	**Maximum Current**
AC Level 1 (1.9 kW)	120 V	16 A
AC Level 2 (19.2 kW)	240 V	80 A
DC Level 1 (19.2 kW)	200 to 450 V	80 A
DC Level 2 (90 kW)	200 to 450 V	200 A

2.3.5. AC-DC and DC-AC Converters for V2G

The V2G system interfaces with the grid through an AC-DC converter system that incorporates a rectifier, a DC-link bus and an inverter, as shown in Figure 4. The grid interface alternates the functions of a rectifier and an inverter depending on its operational mode.

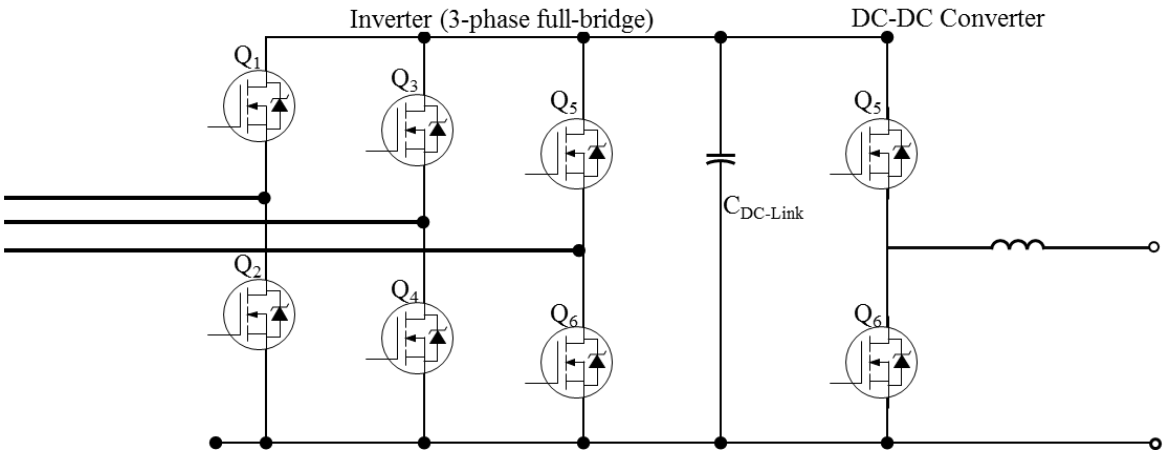

Figure 4. AC-DC converter topology that connects the V2G system with the power grid

While the battery system is being charged, it acts as a DC load fed from the grid through the rectifier. Conversely, if the V2G system is required to provide additional energy to the grid to meet demand peaks, the AC-DC converter subsystem operates as an inverter while the battery system acts as a source, injecting power into the grid via the inverter.

The equations governing three-phase full-bridge rectifiers and inverters have been derived in [18, p. 100 & 300]. In summary:

$$\text{rectifier output,} \quad V_{dc} = \frac{3}{\pi} V_{Lmax}, \tag{2-2}$$

$$\text{inverter output,} \quad V_L = \sqrt{\frac{2}{3}} V_{dc}, \tag{2-3}$$

$$\text{and} \quad V_{Ln} = \frac{4 V_{dc}}{\sqrt{2}n\pi} \sin\frac{n\pi}{3}, \tag{2-4}$$

where V_{dc} is the DC-link voltage, V_L is the three phase AC line RMS voltage with a peak value of V_{Lmax}, n is the harmonic number and V_{Ln} is the RMS value of the nth harmonic line voltage.

V2G charging systems incorporate DC-DC converters, discussed in [19] and [20], that enable coupling of a single DC-link bus to ESS batteries with differing terminal voltages. Often, these are implemented using pulse width modulated (PWM) buck-boost converters.

2.3.6. Harmonic Filtering Methods

The switching operations involved in typical pulse width modulation (PWM) techniques used by power electronic converters introduce harmonics that need to be filtered out prior to injection into the power grid. Various topologies including L, LC and LCL filters have been developed. According to Dursun and Döşoğlu [21], in comparison to the simpler L and LC filters, the LCL filter performs better at lower switching frequencies, has a smaller voltage drop and provides the best damping effect of the three topologies. In [21], they also present a method to calculate the LCL filter circuit parameters for a given inverter DC-link voltage and current capacity.

2.3.7. Converters and Power Grid Interaction

In a typical V2G system, the charger serves as the interface between the vehicle and the grid. It incorporates a voltage regulation subsystem as well as a DC-link capacitor to reduce voltage ripple. A fuzzy-decision-making strategy is proposed in [20] for voltage regulation on the V2G vehicle network and optimization of the DC-link capacitor, while achieving load leveling and variance minimization. It relies, amongst other things, on predictions of vehicle availability, state of charge and iterative estimations of the grid load demand. It suggests an effective method of vehicle network voltage regulation using reactive power compensation. However, the emphasis is on operation over multiple hours, and does not consider transients.

Previous studies of voltage regulation also suggest that control of the voltage, at the point of common coupling of inverters to the grid, is possible by varying the reactive power flow to the power grid [22]. While these are useful means of optimizing system component parameters, they do not address the transient effects in detail.

Wu et al. [23] presented a simulation model of a three-phase PWM charger with V2G capability, which was used to analyze harmonic distortion due to operation of the charger over a 24-hour period. It was demonstrated that total harmonic distortion (THD) had significant rapid variations when chargers switched between charging and discharging modes. While it included a frequency domain analysis of the total harmonic distortion, it did not consider the non-linear time domain transients in detail.

2.4. Chapter Summary

Studies reviewed have focused on ways of optimizing the power flow and regulation on V2G networks. But detailed study of the transients, which are important in the design of resilient equipment for use in future V2G-enabled grids, appears not to have received the same level of attention. This thesis, therefore, examines transient interactions between the power grid and vehicle network as they relate to voltage and load fluctuations.

3. METHODOLOGY

Given the objective to simulate a simplified V2G system for transient studies as well as testing of network load and voltage management algorithms, a logical approach would be to start with a design of the various modules, followed by a phased integration, with intermediate functional testing, until full system integration is achieved.

In designing the modules, two options present themselves. The first possible method is to build the modules with interfaces, using calculated parameter values, and perform integrated testing after all modules are completed and connected. However, this could involve complicated debugging challenges with potential delays. An alternative approach is to test and verify each individual module, to ensure satisfactory performance before integrated testing. The risk with this approach is that it neglects to compensate for variations in module performance under load conditions, which usually requires some refinements in the choice and modeling of parameters. The approach chosen is a balance between the two methods. A top-down process for the design of the V2G system is followed. Individual modules are designed and tested for basic function with respect to theoretical expectations. Then groups of modules are tested for alignment with theoretical projections using waveform measurements for detailed analysis.

An overview of the proposed design is shown in Figure 5. It depicts a simplified distribution-level power grid, an AC/DC converter capable of switching between inverter and rectification modes and a V2G vehicle network incorporating battery management systems and SoC monitoring.

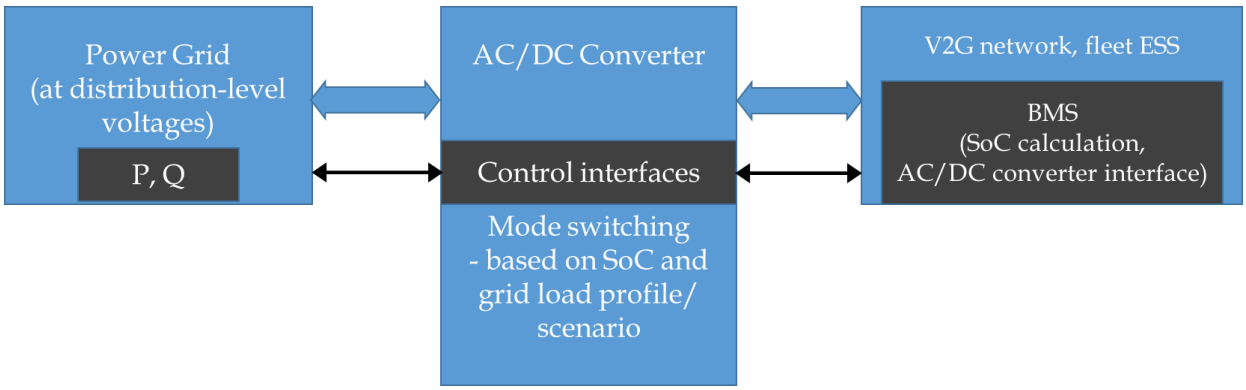

Figure 5. Block diagram of V2G system used for design

3.1. Tools

The primary tool for this study is Simulink®, a software component of MathWorks® R2019b, running on Windows Server 2012. Simulink includes several analysis tools and building blocks for simulating electric grids, three-phase systems, converters of various modes and topologies, renewable power generators and loads. In addition, through the use of Simscape™, subsystem models that combine Simulink blocks with models of physical components are built and tested.

3.2. Data

Part of the data for this study is obtained from manufacturer documentation. Additional data is sourced from referenced research articles. Some vehicle data was obtained from [1]. Also, documentation on IEEE test feeders, [24] & [25] served as a basis for the modeling of the grid component. Some equivalent circuit parameters are estimated using calculations and scaled-up values based on acquired data. In addition, V2G operating profiles have been synthesized to approximate real-world scenarios. Not all the data required was available in the form desired.

For example, the non-linear relationship between terminal voltage and SoC of lithium-based rechargeable PEV batteries was extracted from a built-in Simscape block [26].

3.3. Model Design

The Simulink model shown in Figure 6 represents a V2G system comprising a simplified power distribution grid with a generator, three phase load and transformer, a vehicle ESS network comprising two vehicles, a bi-directional AC-DC converter and the DC-link coupling to the vehicle ESS network.

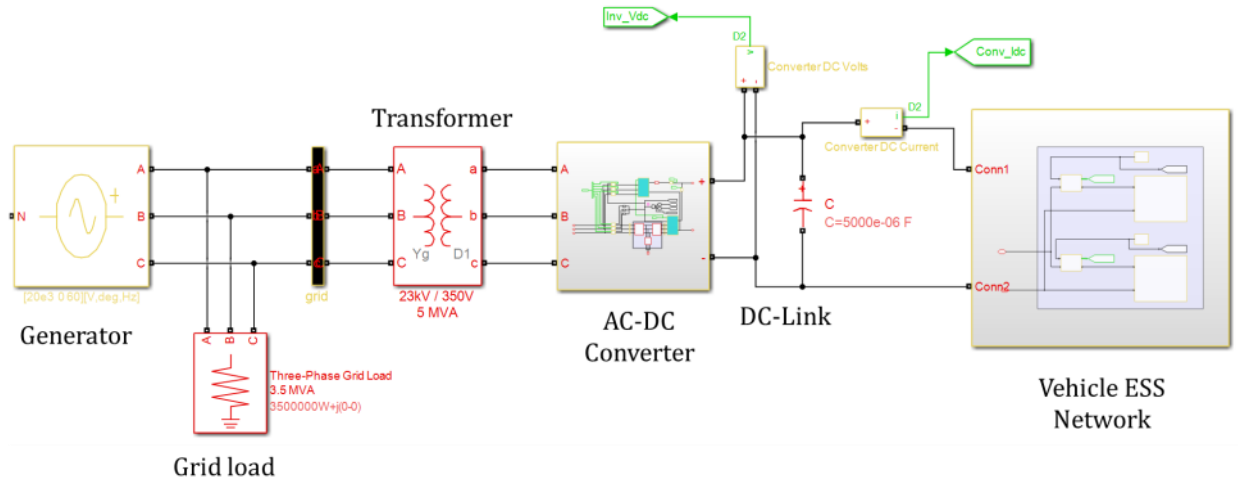

Figure 6. Simulink model of V2G system

3.3.1. Power Grid Model

The modeled power grid is a theoretical three-phase network comprising a three-phase 20 kV, 60 Hz, 5 MVA generator, a three-phase 3.5 MVA load, a bi-directional AC-DC converter and a 5 MVA transformer whose ratio has been chosen to match the voltage levels on the grid with the DC network nominal voltage. Grid synchronization details are not represented in the

model. The emphasis on use of vehicle fleets for load-leveling and peak-shaving coupled with design power levels in the order of megawatts, suggests operations in the mid to high voltages used on a power distribution grid. While other studies have used Node 450 of the IEEE 123-node test feeder [20], and Nodes 650 and 634 of the IEEE 13-node test feeder, which operate at 4.16 kV and 480 V, respectively, this study uses a theoretical grid operating at 20 kV.

3.3.2. Vehicle Fleet ESS Network Model

The vehicle network is modeled as a fleet of two, as shown in Figure 7, with the option to enable or disable either, independently. Each vehicle within the fleet is represented by a battery model, a profile block and switch to connect or disconnect it from the charging network. The switches are triggered using signals from the profile blocks.

Since both vehicles are connected to the same terminals on the bi-directional AC-DC converter, it is not possible to operate one in charging mode while running the other in grid injection mode; the operating mode of the converter determines the direction of power flow for both vehicles, or whichever is plugged in.

The premise of the model design is that a battery SoC must be within acceptable preset limits before the associated vehicle ESS is allowed to participate as a V2G energy source [1, pp. 8, 30]. Thus, the connection of a vehicle to the grid may be overridden by its SoC level, if that falls below a certain threshold. Consequently, the SoC and vehicle connection state are both monitored in the ESS model for use by the bi-directional AC-DC controller logic.

For aggregate vehicle capacity in a real world system, the SoCs of multiple vehicles are considered to determine those that have sufficient charge to be available as sources and those that need to be charged, which will act as loads. Increasing or decreasing the number of vehicles

changes the system capacity subject to satisfaction of SoC constraints. Hence, the SoCs in the model reflect the changes in vehicle aggregate capacity.

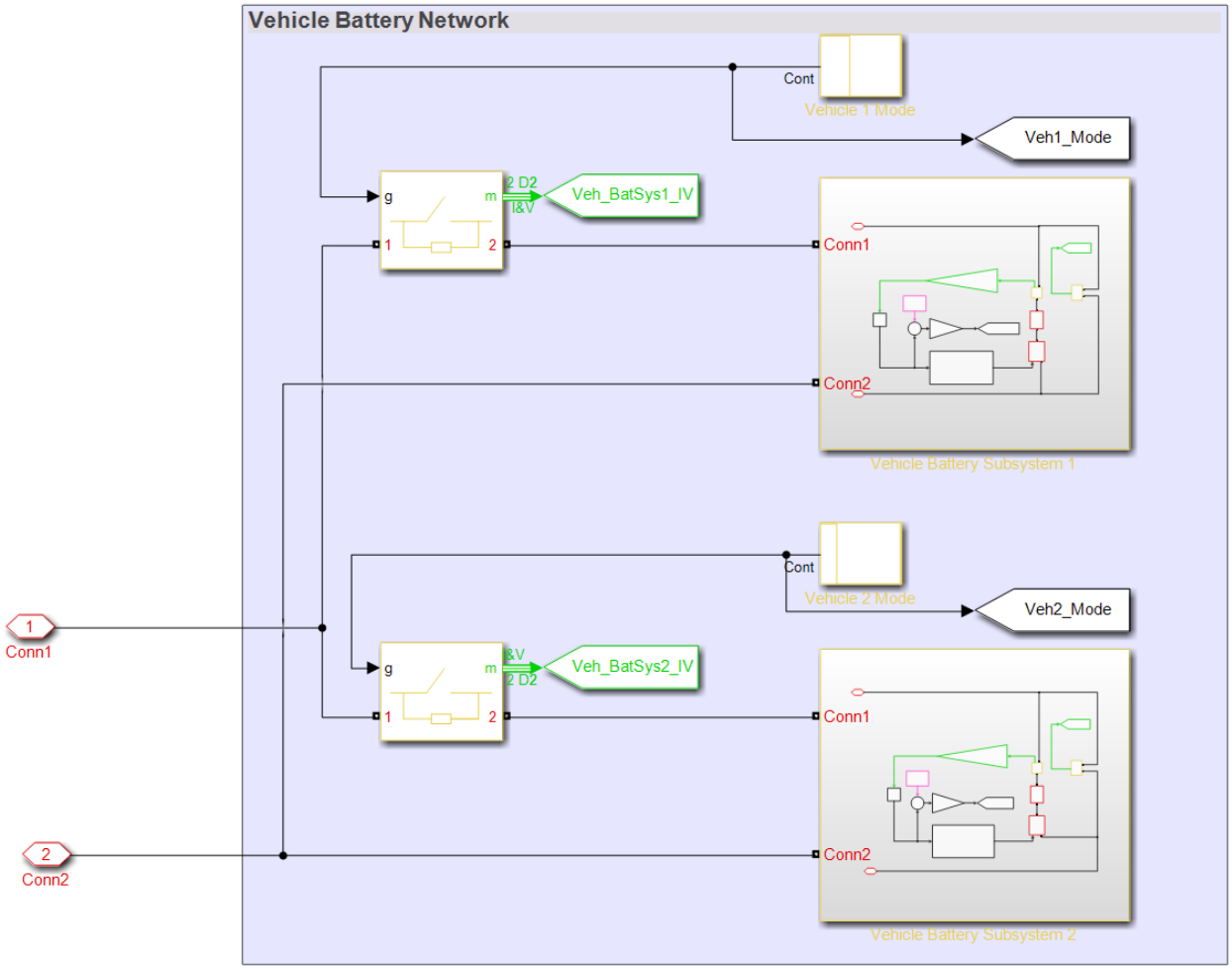

Figure 7. Simulink model of vehicle fleet battery network

3.3.3. Battery Model

A 250 Ah, 350 V Li-Ion battery is modeled for each vehicle. The battery modeling technique applied is described in [4], in which the battery state of charge, *s(t)*, modeled as a function of time for an initially fully charged battery, may be represented by the equation:

$$s(t) = 1 - \frac{i_d t}{C_v} \ , \qquad (3\text{-}5)$$

where i_d is a constant discharge current, t is time and C_v is the available battery capacity as a function of i_d *[4]*. It is clear that this is a variation of equation (2-1).

This relationship is used to calculate battery state of charge and is dependent on knowledge of the battery nominal capacity. In addition, the voltage vs. amp-hour characteristics of the battery are necessary to estimate terminal voltages.

A generic Simscape™ rechargeable battery [26] is configured with parameter values from a known Tesla automobile Li-ion battery [15]. Each battery model within the vehicle fleet model in Figure 7 uses a Thévenin equivalent of the battery, in combination with a non-linear mapping of voltage to SoC, to estimate the instantaneous battery voltage. A one-dimensional lookup table block is used for modeling the non-linear relationship between the battery terminal voltage and its state of charge. To obtain the voltage vs. amp-hour profile for the 350 V battery used in the model, modifications are made to the Simscape built-in block [26], voltage vs. amp-hour graphs are generated, and data points extracted to create the look-up table used in the design of the battery model. Figure 8 shows the resulting profiles at different discharge currents and the battery operating regions. Due to the much shorter time intervals of the transients relative to natural temperature changes, the effects of temperature on the battery SoC are considered negligible for this model.

Having established voltage vs. amp-hour profiles for the vehicle batteries, the terminal voltages can be derived from a calculation of the SoCs. To obtain the SoC, the simulation computes the residual charge in each battery using its net current flow.

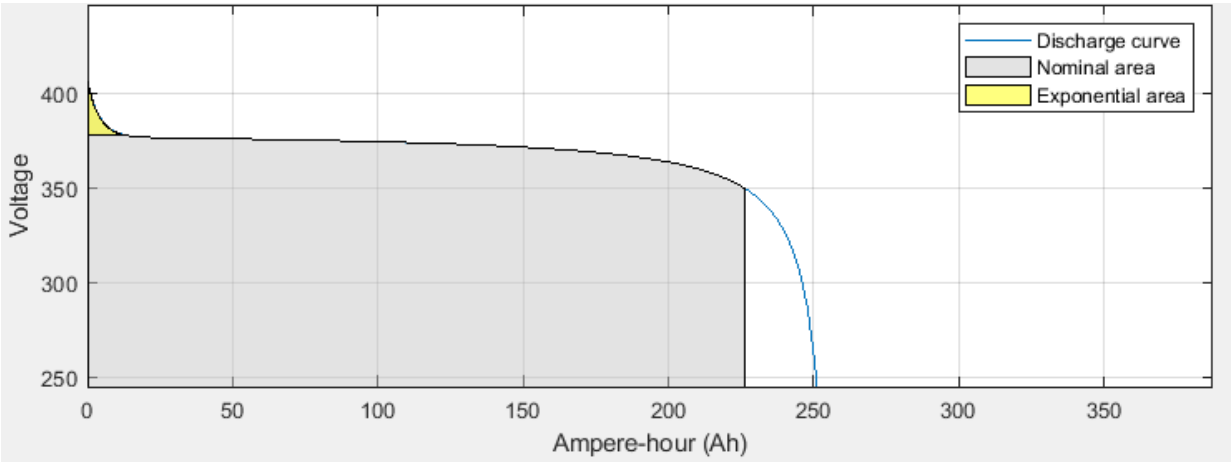

(i)

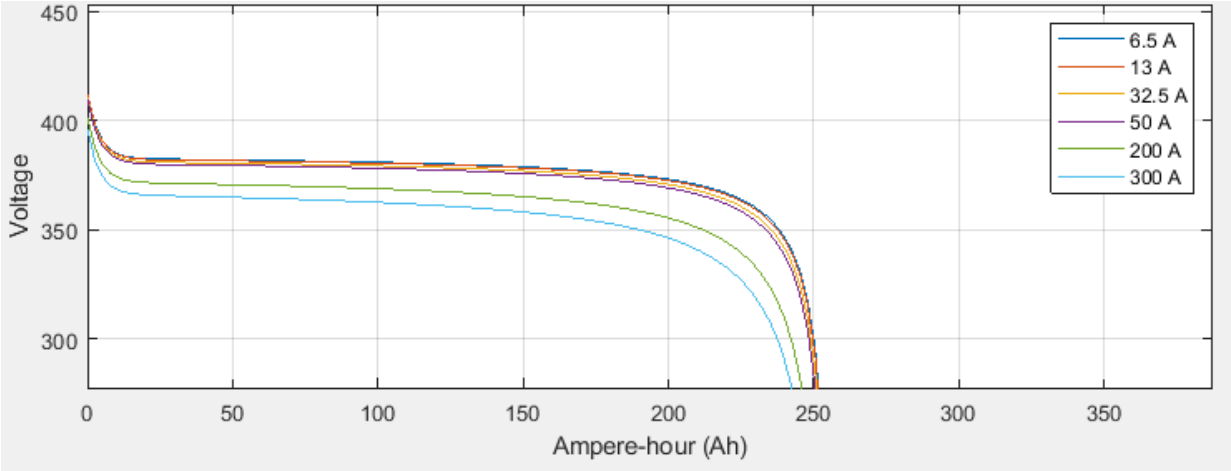

(ii)

Figure 8. Voltage-amp hour characteristics for the 350 V, 250 Ah model battery showing (i) operating regions and (ii) profiles for different currents

In order to model the bi-directional nature of the battery current and account for the charge levels, the Thévenin equivalent of the battery [26] is modified as shown in Figure 9, and a signal feedback incorporating an integrator is added to accumulate the current flow into charge flow units, for determining the residual battery charge. As shown in the "Gain_Chg_Step" gain block, the integrator block gain is adjusted by a value of 9000 – obtained by measuring the rate

of charge and discharge at a constant current value – to ensure that the dynamics during simulation accurately represent equation (3-5). It is worth noting that changes to the simulation step-time require further adjustments to the integrator gain to maintain accuracy.

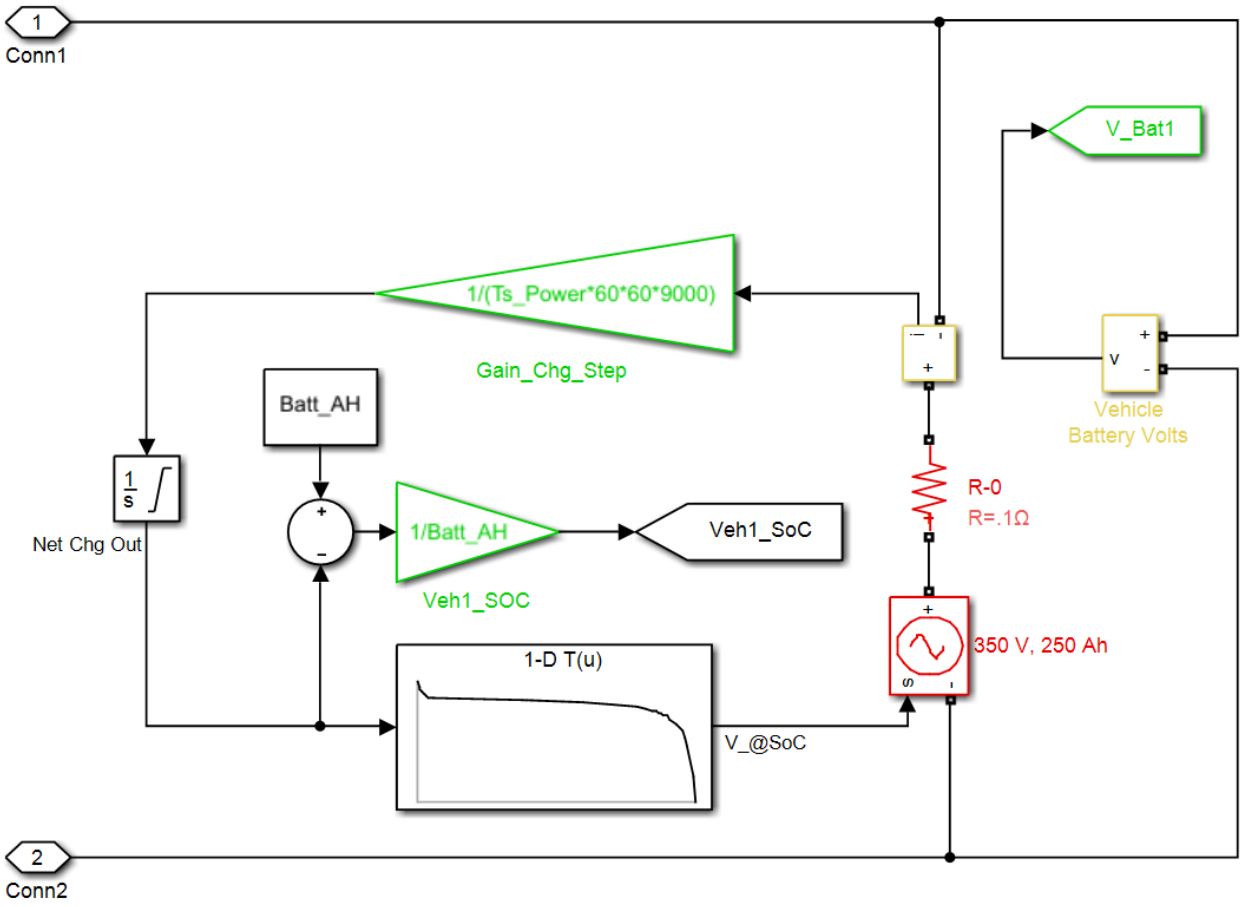

Figure 9. Simulink model of battery featuring Thévenin equivalent, integrator loop and one-dimensional (1-D) lookup table block for SoC calculation

3.3.4. Bi-directional AC-DC Converter

The bi-directional AC-DC converter transfers power to and from the vehicle fleet depending on the mode of operation selected. In a physical implementation, a service provider, working with an aggregator, schedules vehicles for charging or peak power supply using

information such as driver or vehicle operational cycles, vehicle SoCs and other signals from the BMS [1]. In this model, the bi-directional AC-DC converter shown in Figure 10 is designed as an integrated rectifier and inverter, and configured such that either subsystem is isolated from the power grid while the other is in operation. A system of interlocking switches in the model ensures that the inverter and rectifier subsystems operate mutually exclusively; the three-phase double-pole mutually exclusive switch has been constructed using six ideal switch blocks and is necessary to prevent the inverter and rectifier from operating simultaneously on the power grid. This eliminates the risk of feedback from the rectifier output to the power grid via the inverter.

For simplicity, the transformer turns ratio is chosen to eliminate the need for a DC-DC converter. From equation (2-2), a sinusoidal 300 V RMS line voltage input to the three-phase rectifier would produce a DC output voltage of:

$$\frac{3}{\pi} \text{ x } 300\sqrt{2} \;=\; 405.1 \text{ V},$$

which is sufficient to charge the batteries.

Also, from equation (2-3), a 400 V DC input to a three-phase full-bridge inverter would produce an RMS AC voltage of :

$$400 \text{ x } \sqrt{\frac{2}{3}} = 326.6 \text{ V (RMS)}, \text{ having a fundamental of } 311.9 \text{ V (RMS)}.$$

It is worth noting that the power transformer turns ratio results in a voltage transformation from 20 kV to 304.3 V at high and low voltage sides, respectively.

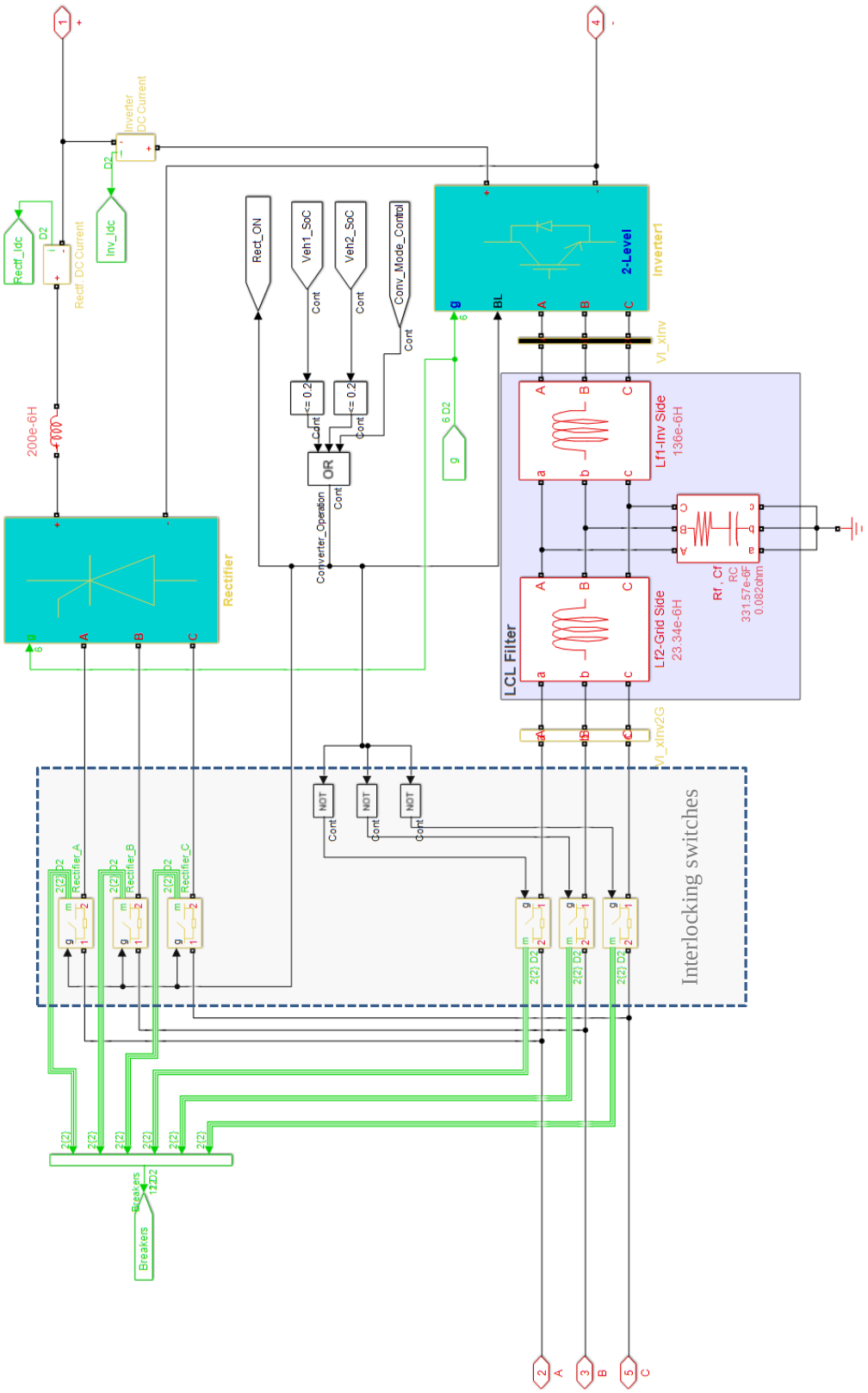

Figure 10. Simulink model of bi-directional AC-DC converter sub-system

The sinusoidal reference signals for the gate control (U_{abc}), shown in Figure 11, ensure the correct thyristor firing sequence for both rectifier and inverter, and also synchronizes them in the model.

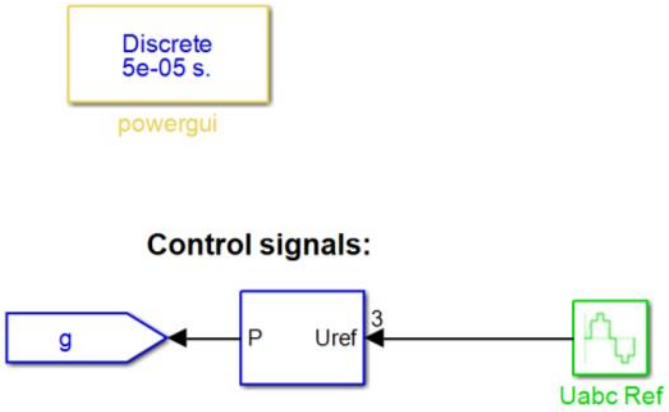

Figure 11. Control signal for AC-DC converter PWM switch control

3.3.5. Inverter LCL Filter

The output of the inverter is a two-level, PWM waveform with a sinusoidally modulated duty-cycle, shown in the first of the four plots in Figure 12. Its harmonic content makes it unsuitable for direct injection to the power grid. Thus, an LCL filter is used to reduce the harmonics at the inverter output. In [21], a set of equations is developed for calculating the values of inductance and capacitance in an LCL filter using the DC-link voltage, capacity and current ripple as reference bases. Applying the ratios proposed to the ratings gives the values for inductances and capacitances listed in Table 2. The key values of interest from Table 2 are filter capacitance (C_f), capacitor series resistance (R), inverter-side LCL filter inductance (L_{f1}) and grid-side LCL filter inductance (L_{f2}). The output of the inverter is substantially improved after passing it through the LCL filter. The waveforms presented in Figure 13 show the LCL filter output expanded over one cycle of the power grid voltage.

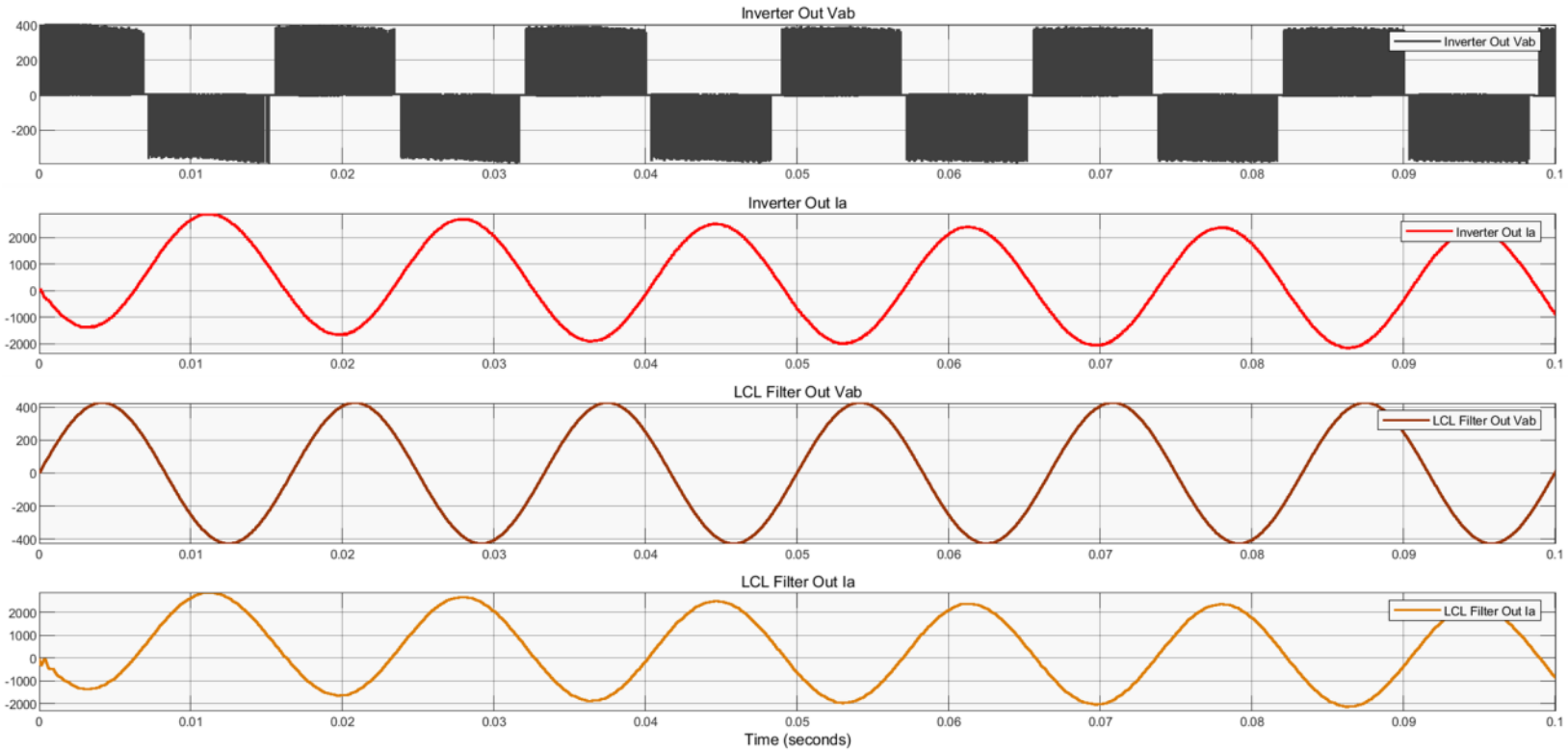

Figure 12. Inverter voltage and current outputs for time = 0 – 0.1 s, measured before and after LCL filtering, with L_{f2} = 136 µH, L_{f2} = 23.34 µH, R_f = 0.082 Ω and C_f = 331.57 µF

From top to bottom: (i) inverter output line voltage (Vab), (ii) inverter phase A current output (Ia), (iii) LCL filter output line voltage (Vab) and (iv) LCL filter phase A current output (Iab).

Table 2. Inverter parameters including calculated values of inductance and capacitance for the LCL filter (based on formulae in [21])

Parameter	Given/Calculated Value	Design Value
DC Current Capacity (ESS in two vehicles)	1000 A	1000 A
DC-Link Voltage (inverter RMS)	400 V	400 V
Power Output	400 kW	400 kW
$I_{max\text{-}line}$	1414.2136 A	1414.21 A
I_{max} (phase current)	816.4966 A	816.50 A
Δ-I_{max} (ripple current, 10% phase)	81.6497 A	81.65 A
f_g (Grid frequency)	60 Hz	60 Hz
Lower limit of filter frequency to avoid resonance (10 f_g)	600 Hz	600 Hz
Switching Frequency (f_{sw})	6000 Hz	6000 Hz
High limit of filter frequency up to avoid resonance (f_{sw} /2)	3000 Hz	3000 Hz
LCL Resonant Frequency (10 f_g < f_{res} < f_{sw} /2)	1958.088 Hz	2000 Hz
Filter Capacitor (C_f)	331.5728 μF	331.57 μF
Inverter-side filter inductance (L_{f1})	136.0828 μF	136 μF
Grid-side filter inductance (L_{f2})	23.3427 μF	23.34 μF
R (capacitor series resistor)	0.081712 Ω	0.082 Ω
Attenuation factor (k_a)	0.1	0.1

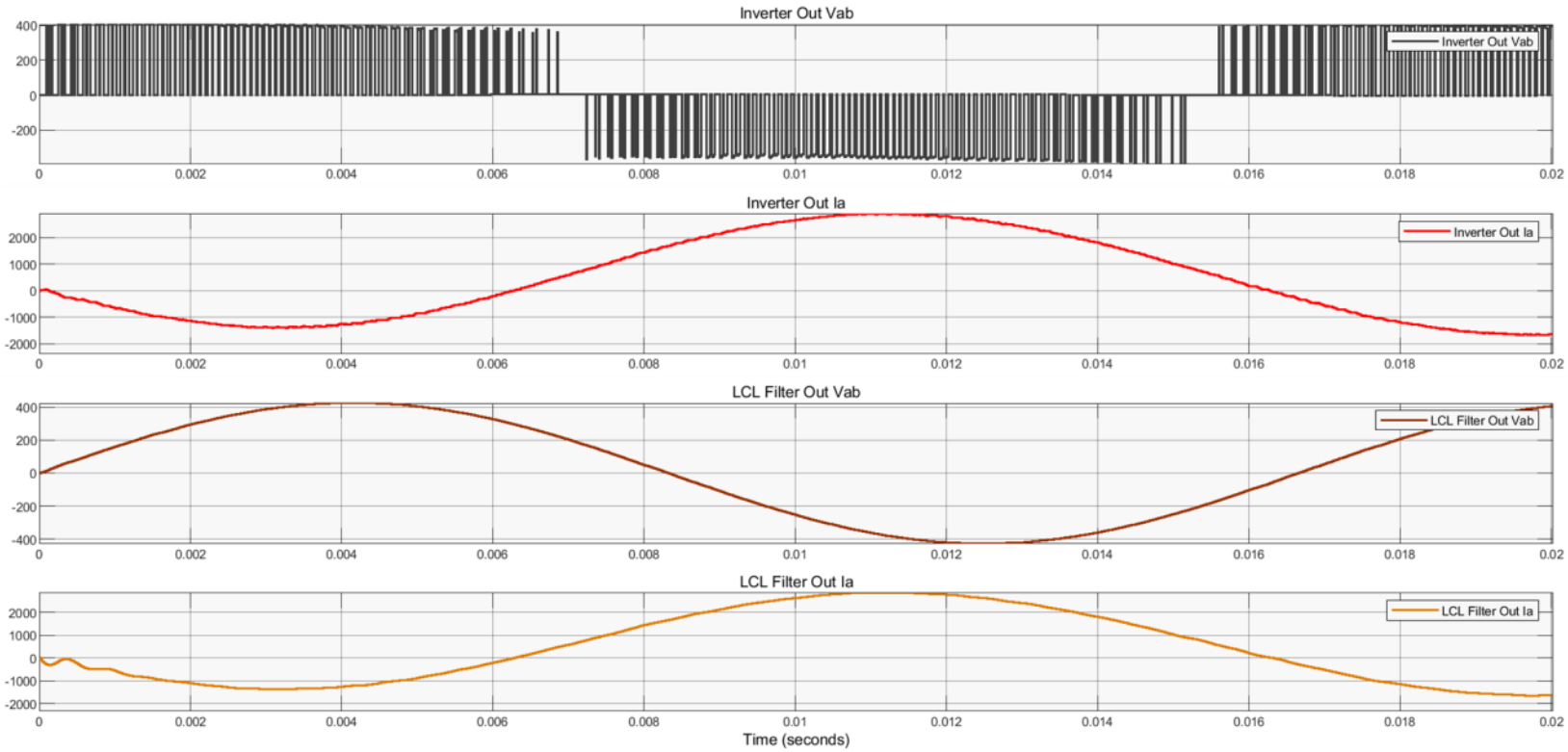

Figure 13. Inverter voltage and current outputs expanded for time = 0 – 0.01 s, measured before and after LCL filtering, with L_{f1} = 136 µH, L_{f2} = 23.34 µH, R_f = 0.082 Ω and C_f = 331.57 µF

From top to bottom: (i) inverter output line voltage (Vab), (ii) inverter phase A current output (Ia), (iii) LCL filter output line voltage (Vab) and (iv) LCL filter phase A current output (Iab).

3.3.6. V2G Model Controller

The control scheme adopted in this V2G model is based on limit triggers. Simulink stair generator blocks are used for synthetic generation of profile changes in converter mode (inverter or rectifier) and vehicle plug-in state (availability) at predetermined points in time. The converter modules are designed with interfaces that read these state sequences during simulation.

In a practical system, the variables of interest are the grid AC voltages, real and reactive power, battery states of charge, the DC voltage at the converter point-of-coupling with the vehicle battery energy storage system, and DC charging currents. Within the BMS, temperature is also considered in the regulation of charging currents. However, in this model, the variables of interest are the grid AC voltages and currents, the battery states of charge, the DC voltages and charging currents. Temperature is not considered. A primary objective in a V2G system is to maintain battery SoCs within a set range. The SoC is monitored for each battery in the model and if either falls below a threshold of 0.2, the system inhibits further charge depletion and switches into charging mode by turning on the rectifier and simultaneously turning off the inverter. Given the relatively slow rate at which SoCs change compared with the transient changes being studied, this scenario seldom presents itself in this study.

3.3.6.1. Converter Operational Mode Signals

The operation of the converter is controlled using a sequence of states from a stair generator block. This is similar in function to the role of a V2G service coordinator. The output of the block is a binary “Conv_Mode_Control” signal:

‘1’ signals “rectifier” or “vehicle charging mode”, and

‘0’ signals “inverter” or “grid injection mode”.

In a vehicle charging scenario, vehicles are treated as loads and used for load leveling during periods when energy demand on the power grid is low. During peak periods, the V2G network is required to inject additional power into the grid, in which case the signal "Conv_Mode_Control" is set to '0'.

3.3.6.2. Vehicle Availability Signals and SoC

Another issue of concern with V2G capacity is the availability of vehicles. This is modeled using changes in vehicle plug-in state. The presence of each vehicle is indicated using binary profile signals, "Veh1_Mode" and "Veh2_Mode", from two stair generator blocks labeled "Vehicle 1 Mode" and "Vehicle 2 Mode", respectively. The signals assume two states:

'1' signals vehicle "connected" or "plugged-in", and

'0' signals vehicle "disconnected" or "not-plugged-in".

Hence, changes in vehicle availabilities are accounted for by changing the signal output from the stair generators in the model.

3.4. Model Summary

The resulting model is one in which the vehicle network draws power from, injects power to, or does nothing to the grid, depending on the operating mode of the converter and the availability of plugged-in vehicles.

By altering the "operating mode" profile fed to the bi-directional converter via the "Conv_Mode_Control" signal and simultaneously feeding "vehicle connection" profiles through the "Veh1_Mode" and "Veh2_Mode" signals, it is possible to simulate scenarios with varying battery charging loads while simultaneously altering the direction of power flow on the grid.

4. RESULTS AND DISCUSSION

In this chapter, the V2G model simulation and test data are presented. Two test scenarios are presented, each detailing test objectives and inputs along with results. An overview of each set of results is supplemented by more detailed discussions focusing on the transients.

4.1. Test Model Description

With reference to Figure 6, the model may be considered as comprising three sections – (i) power grid, (ii) bi-directional AC-DC converter with DC-link capacitor, and (iii) vehicle fleet. As shown in Figure 14, the three-phase power generator injects real and reactive power into the grid. The power is delivered to a three-phase 3.5 MVA load and a transformer, which steps down the voltage for connection to the bi-directional converter, through which the vehicles are connected to the grid. The load represents consumer demand on a physical grid.

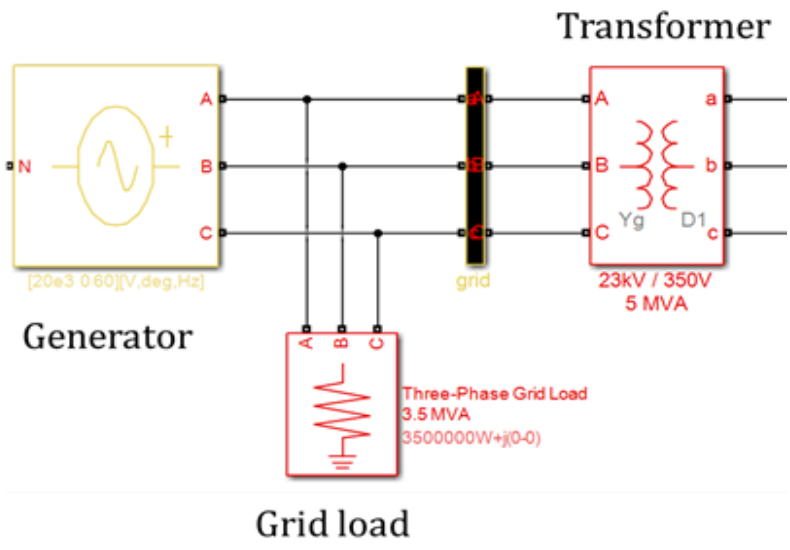

Figure 14. Power grid section of the V2G Simulink model

The bi-directional AC-DC converter, previously shown in Figure 10, changes its mode of operation in response to “Conv_Mode_Control” signals, which are set to ‘1’ or ‘0’ by Simulink stair generator blocks, such as the one labeled “Converter Mode Profile” in Figure 15.

Figure 15. Simulink signal generation for converter operational mode control

The vehicle plug-in states are determined by similar binary signals from vehicle-mode stair generator blocks. Figure 16 shows “Vehicle 1 Mode”, one of two vehicle-mode blocks in the fleet. The interpretations of the control signals are detailed in sections 3.3.6.1 and 3.3.6.2.

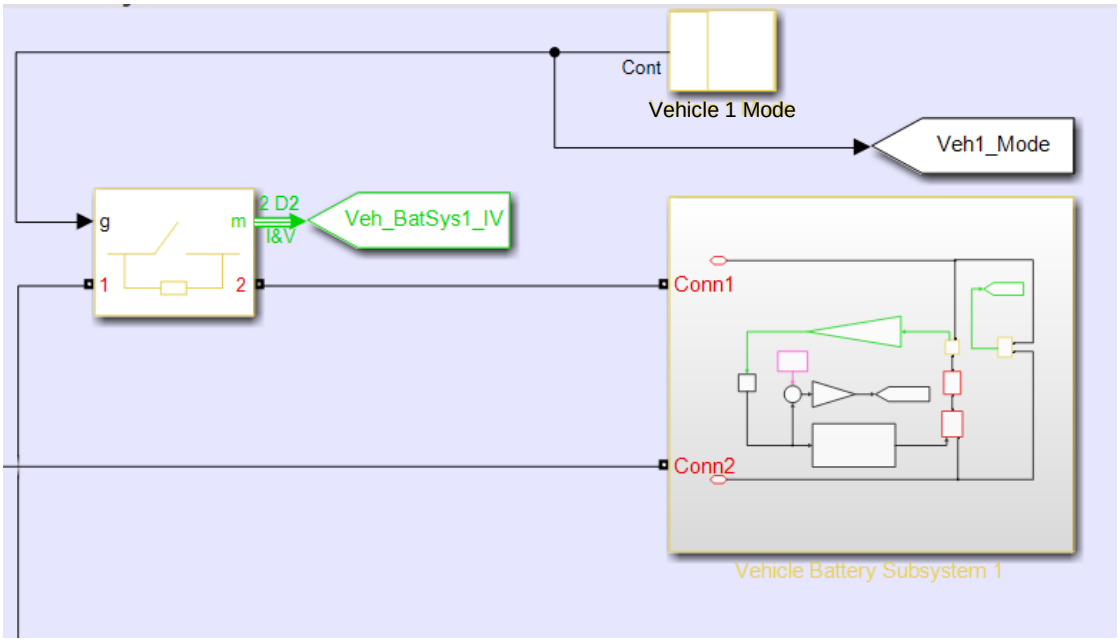

Figure 16. Section of vehicle fleet model showing Vehicle 1 Mode selector arrangement

4.2. Test Setup

The tests are designed to present the system reaction to variations in vehicle battery charging load (through modifications to the number of plugged-in vehicles) and changes in the direction of power flow between the grid and the vehicle fleet network. During simulation runs, the operational modes of the bi-directional AC-DC converter and the plug-in states of vehicles are synthetically controlled using profiles fed from the Simulink stair generator blocks described in section 4.1. The stair generator blocks are configured to produce sequences of states that represent the availability of vehicles (plug-in states) as well as the operating mode of the vehicle charging stations, i.e., "vehicle charging" or "grid injection" modes. The timing of the state changes are chosen to provide information regarding interactions between various system components as synthesized mode changes occur.

The three-phase power grid generator voltage is set at 20 kV for all simulation runs. Vehicle battery terminal voltages vary depending on the direction of power flow. Both vehicle batteries have initial SoCs of 1.0, the maximum value, and preset minimum threshold SoCs of 0.2 for simulation runs. Waveforms are obtained for the power grid AC voltages and currents, vehicle network DC voltages and charging currents, and vehicle battery SoCs.

4.3. Test Scenarios

4.3.1. Test 1: Vehicle to Grid Power Injection with Maximum Vehicle Availability

The purpose of this test is to validate the stable operation of the V2G model in grid injection mode with both vehicle batteries initially fully charged and supplying power to the grid. The converter is started in rectifier (vehicle charging) mode, to enable capturing of transients at

the start of grid injection, then switched to inverter mode after 0.5 s and held in that mode for 10.5 s. Table 3 describes the profile compositions and Figure 17 shows the profile time plots, shown from 't' = 0 – 1 s, since no further profile changes are introduced after 0.5 s.

Table 3. Signal profiles for Test 1

Signal	Vector / Value	Comment
Vehicle Modes 1 & 2	[1, 1]	Both cars plugged in from start to finish
Minimum SoC	0.2, 0.2	For Vehicles 1 & 2
Converter Mode	[1, 0]	Switch to inverter at 2nd sequence step
Time Vector	[0, 0.5]	Units in seconds

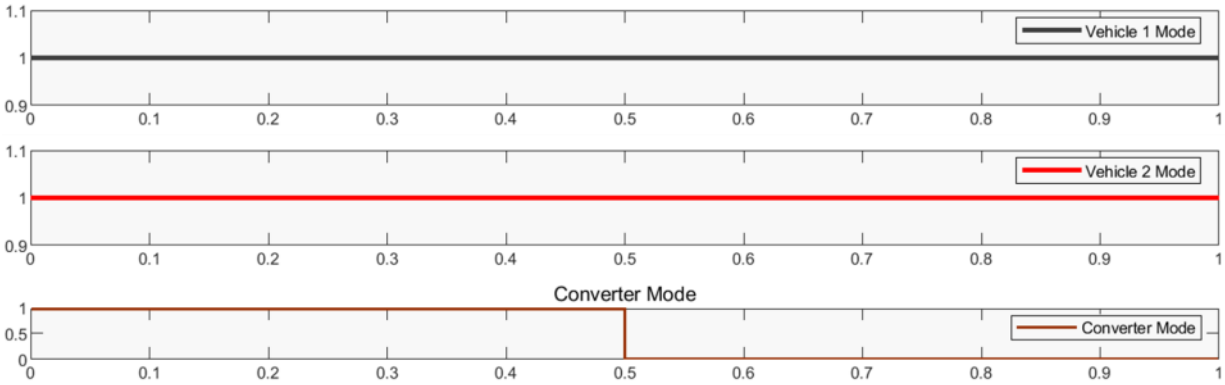

Figure 17. Signal profile plots for Test 1 – for converter: 0 = grid injection & 1 = vehicle charge; for vehicles: 0 = disconnected & 1 = connected

The converter AC and DC voltage waveforms are presented in Figure 18, which shows the gradual reduction in battery terminal voltages in Figure 18.(v). This is an indication of reduction in SoCs, as should be expected in grid injection mode.

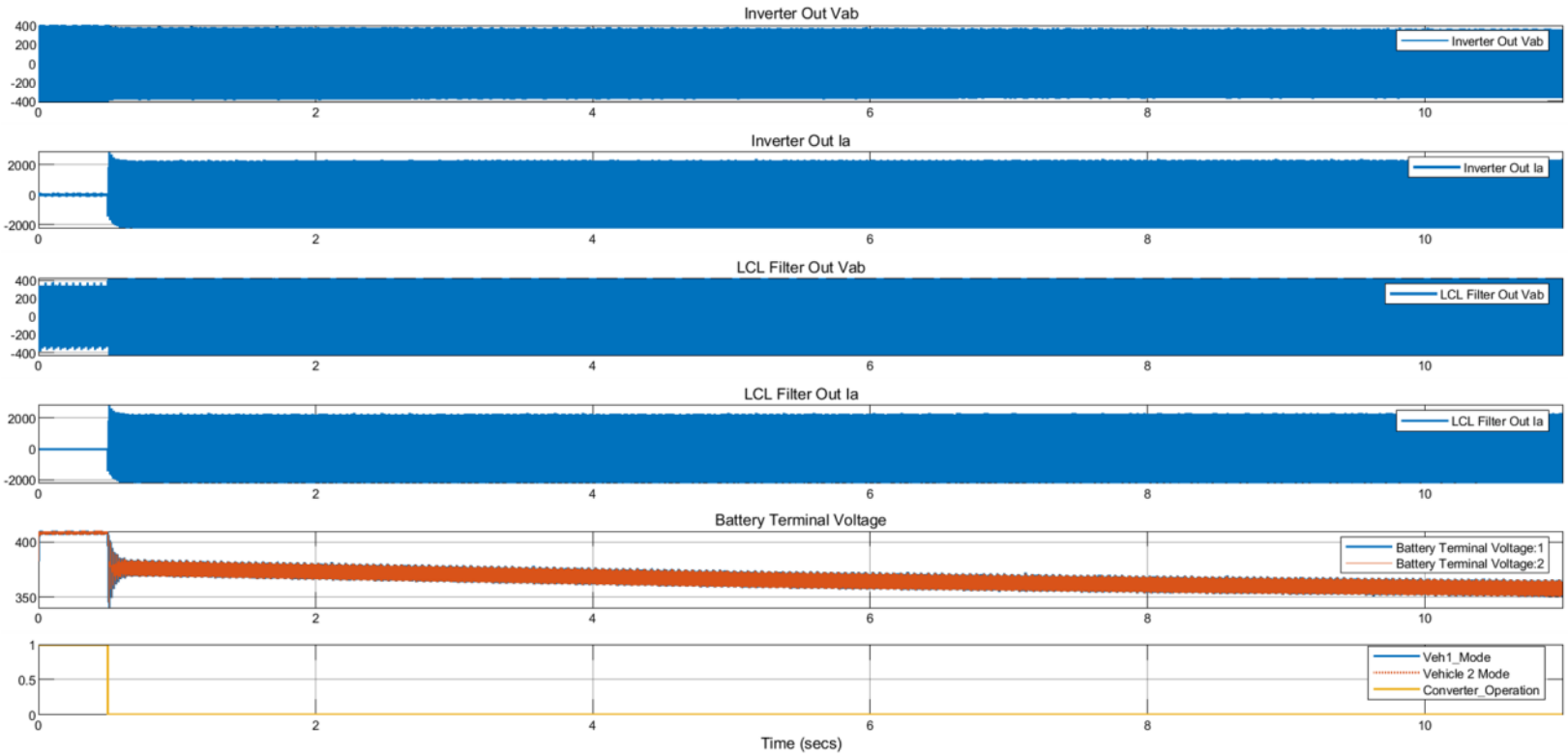

Figure 18. Plots, from time = 0 – 11 s, of inverter and LCL filter Phase A output voltages and currents, vehicle battery terminal voltages, plug-in modes, and converter operating mode

From top to bottom: (i) inverter Phase A output voltage, (ii) inverter Phase A output current, (iii) LCL filter Phase A output voltage, (iv) LCL filter Phase A output current, (v) Vehicles 1 & 2 battery terminal voltages on same axes, (vi) Vehicle 1 & 2 plug-in modes, and converter operating mode on same axes

A more detailed set of the same plots, focusing on the transient region (around t = 0.5 s), is shown in Figure 19. It can be seen how the battery terminal voltage is initially held at about 409 V DC, because the SoC is at 1.0 and the battery voltage is in its exponential region (ref. Figure 8.(i)). There is a slight ripple due to the effects of rectification and the DC link capacitor. At 0.5 s, the ripple voltage becomes more pronounced as a result of the inverter PWM switching. Also, the voltage drops sharply to the battery nominal value and takes about 7 cycles to settle down to its steady-state value in grid injection mode. The harmonic distortion as a result of the inverter switching continues to appear even in steady-state operation. Another point worth noting is the effect of the LCL filter, which smoothens out the PWM waveform in Figure 19.(i) to give the much more sinusoidal output in plot Figure 19.(iii).

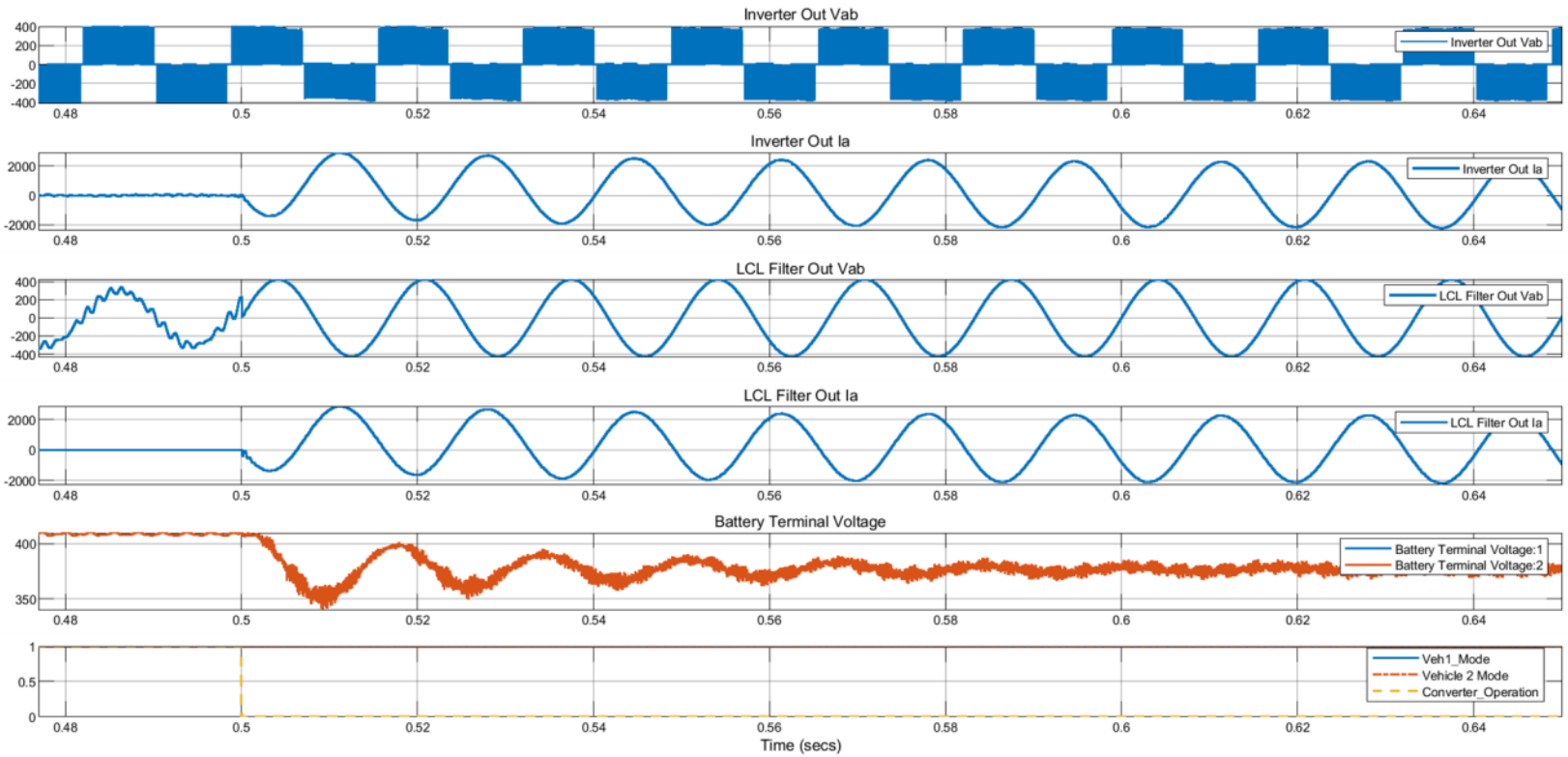

Figure 19. Expanded plots, from time = 0.48 – 0.64 s, of inverter and LCL filter Phase A output voltages and currents, vehicle battery terminal voltages, plug-in modes, and converter operating mode

From top to bottom: (i) inverter Phase A output voltage, (ii) inverter Phase A output current, (iii) LCL filter Phase A output voltage, (iv) LCL filter Phase A output current, (v) Vehicles 1 & 2 battery terminal voltages on same axes, (vi) Vehicle 1 & 2 plug-in modes, and converter operating mode on same axes

Further details are shown in Figures 20 to 23, which expand the plots around the mode transitions. Figure 20 shows the currents in the converter subsystems – the inverter in Figure 20.(i) and rectifier in Figure 20.(ii) – and their combined effect in the converter output in Figure 20.(iii). The significant rectifier current ripple is smoothened by the DC link capacitor at the converter output. Figure 20.(iv) also shows the gradual reduction in SoC as energy is drawn from the vehicle batteries. The battery terminal voltage waveform in Figure 20.(v) is similar to the converter output, as expected. The transient oscillations from 't' = 0.5 – 0.65 s are as a result of the mode transition in the converter from vehicle charging mode to grid injection mode. Figure 21 shows the transients in finer detail from 't' = 0 – 0.01 s and reveals the 360 Hz ripple caused by the operation of the six switches in the three-phase full-bridge rectifier connected to the 60 Hz power grid. Figure 22 expands the plots from 't' = 0.46 – 0.7 s to provide additional detail and reveals that the transient at the transition to grid injection mode, from 't' = 0.5 – 0.65 s, oscillates at about 60 Hz. Superimposed on this are ripples from the switches in the three-phase full-bridge rectifier.

Finally, Figure 23 shows the waveforms at the connection between the inverter and the power grid. It shows the increase in inverter – and LCL filter – output when the converter switches to grid injection mode. This agrees with the expectations based on the design choices in section 3.3 and is further supported by calculations using equations (2-2) and (2-3). However, the current waveforms suggest the presence of a transient DC component during the transition from vehicle charging to grid injection mode.

This test confirms that the V2G system remains stable in grid injection mode while delivering a current of 2000 A (peak) or about 1414 A (RMS), which is the rated capacity listed in Table 2. It also reveals the existence of a transient DC component in the inverter output.

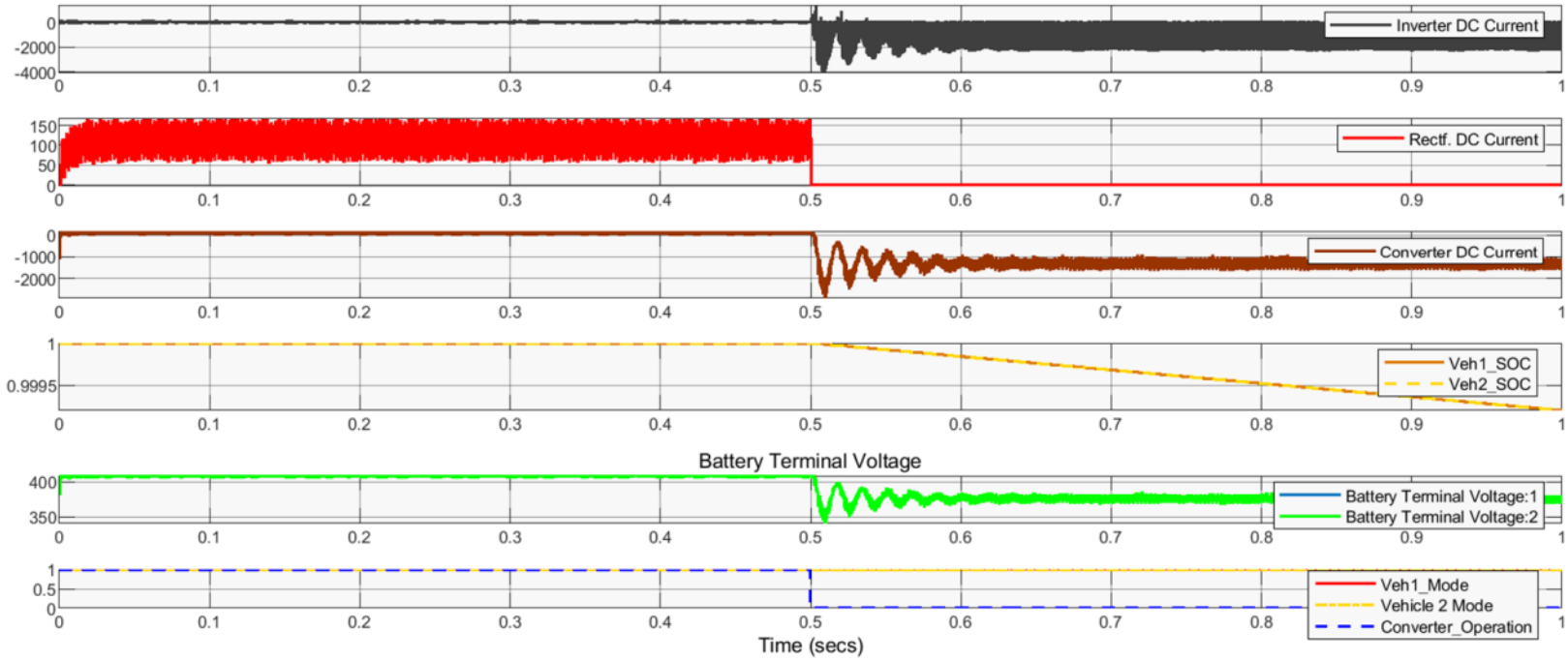

Figure 20. Plots, from time = 0 – 1 s, of V2G grid power injection with two vehicles plugged in

From top to bottom: (i) inverter DC current, (ii) rectifier DC current, (iii) converter DC current, (iv) Vehicles 1 & 2 SoCs on same axes, (v) Vehicles 1 & 2 battery terminal voltages on same axes, (vi) Vehicle 1 & 2 plug-in modes, and converter operating mode on same axes

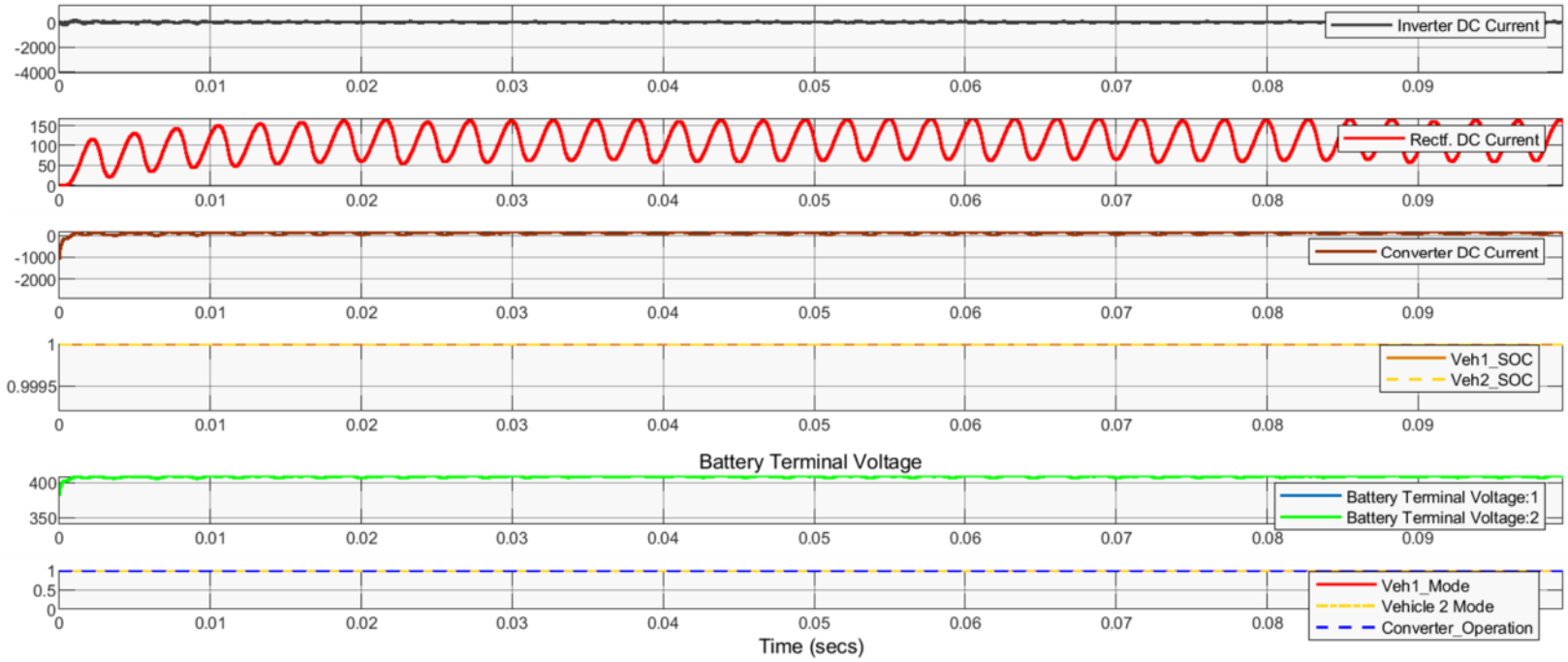

Figure 21. Plots of V2G grid power injection operation, expanded to show initial transients in detail from time = 0 – 0.01 s

From top to bottom: (i) inverter DC current, (ii) rectifier DC current, (iii) converter DC current, (iv) Vehicles 1 & 2 SoCs on same axes, (v) Vehicles 1 & 2 battery terminal voltages on same axes, (vi) Vehicle 1 & 2 plug-in modes, and converter operating mode on same axes

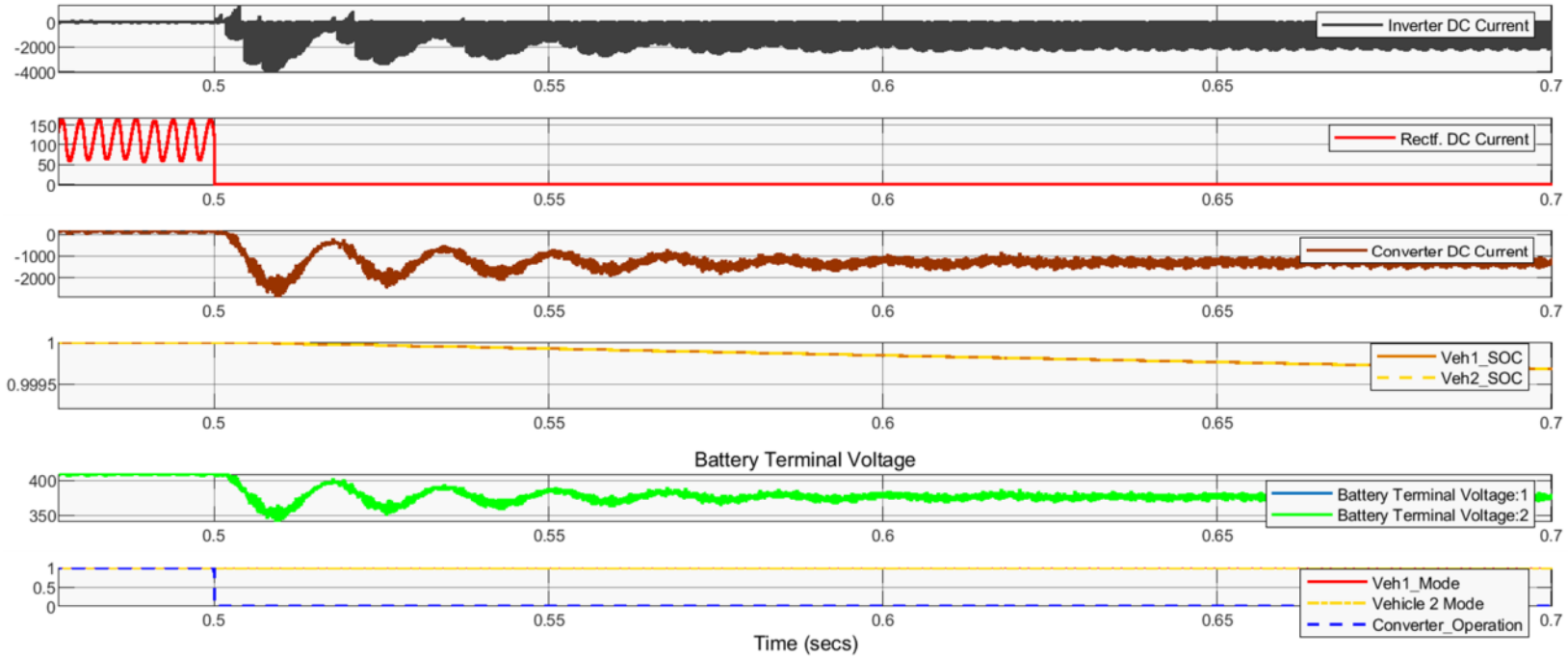

Figure 22. Plots for grid injection, expanded from time = 0.48 – 0.7 s, showing converter subsystem currents during transition to grid injection mode

From top to bottom: (i) inverter DC current, (ii) rectifier DC current, (iii) converter DC current, (iv) Vehicles 1 & 2 SoCs on same axes, (v) Vehicles 1 & 2 battery terminal voltages on same axes, (vi) Vehicle 1 & 2 plug-in modes, and converter operating mode on same axes

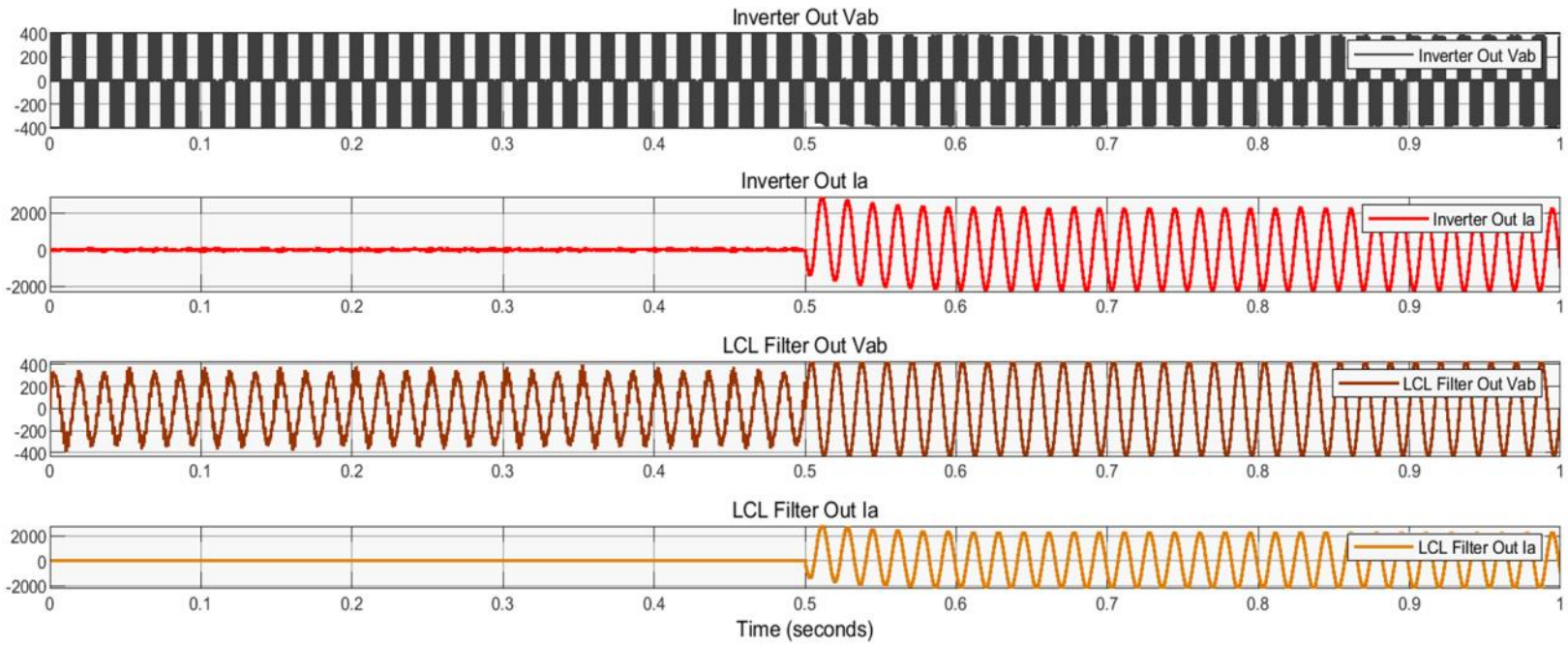

Figure 23. Plots for grid injection, from time = 0 – 1 s, showing inverter voltages and currents injected to the grid before and after LCL filter

From top to bottom: (i) inverter output line voltage (Vab), (ii) inverter phase A current output (Ia), (iii) LCL filter output line voltage (Vab) and (iv) LCL filter phase A current output (Iab)

4.3.2. Test 2: Vehicle Charging with Varying Vehicle Availability

In this test, the vehicle network operates as a variable charging load while the effect of those variations on voltages and currents at various nodes of the system are observed. Again, to enable capturing of transients at the start of vehicle battery charging, the bi-directional AC-DC converter is started in grid injection (inverter) mode.

Initially, both vehicles are plugged in and have battery SoCs of 1.0. After 0.15 s, the converter is switched to rectifier mode. At this point in time, both vehicle batteries are being charged. At 't' = 0.3 s, Vehicle 1 is "unplugged" and left unplugged for 0.9 s. Vehicle 2 is later unplugged at 't' = 0.5 s and held in that state until 't' = 1.5 s. The profile data is summarized in Table 4 and plotted in Figure 24.

Table 4. Signal profiles for Test 2

Signal	Vector / Value	Comment
Vehicle Modes 1 & 2	[1, 0, 1,]	Cars initially plugged, then unplugged and plugged back
Vehicle 1 Time Vector	[0, 0.3, 1.2]	Unplugged at 0.3 s, plugged back at 1.2 s
Vehicle 2 Time Vector	[0, 0.5, 1.5]	Unplugged at 0.5 s, plugged back at 1.5 s
Converter Mode	[0, 1, 1]	Switch to rectifier mode at 2nd sequence step
Converter Time Vector	[0, 0.15, 2]	2nd sequence step at 0.15 s

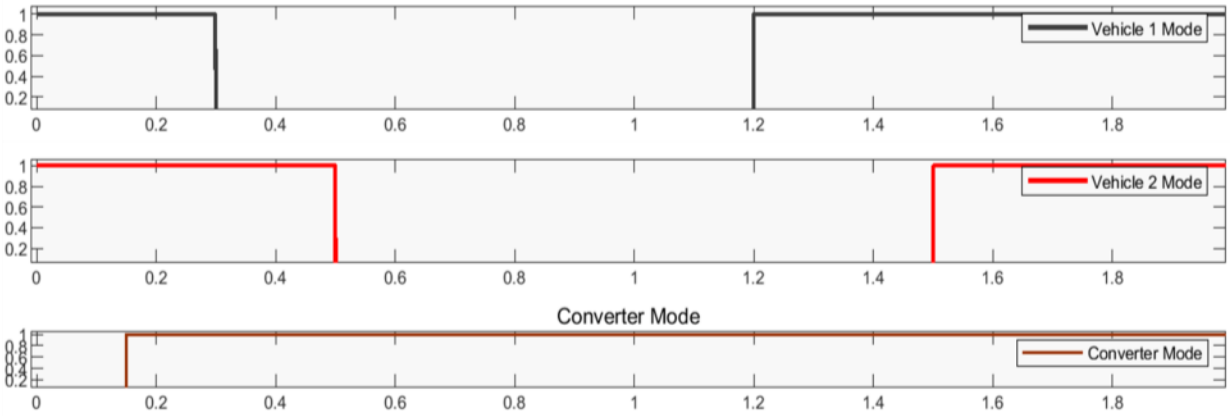

Figure 24. Signal profile plots for Test 2 – for converter: 0 = grid injection & 1 = vehicle charge; for vehicles: 0 = disconnected & 1 = connected

First, measurements at the same nodes as in Test 1 are taken and shown in Figure 25. As expected, output currents of the inverter and LCL filter – Figure 25.(ii) & (iv) – are zero during rectifier operation. However, there is a ripple voltage due to the PWM switching operation in the converter. During rectification, the inverter is isolated only from the power grid; its DC input shares the same port as the rectifier DC output, thus it still produces a PWM voltage.

The battery terminal voltages have noticeable ripple (3 – 6 V peak-to-peak) as a result of the ripple from the rectifier. Also, the ripple voltage appears to decrease at the converter terminals as battery load is increased, as evidenced by the decreased ripple from 't' = 0.15 to 0.3 s, and after 't' = 1.5 s. This is shown more clearly in Figure 26.(iii) & (v). Having more batteries in parallel appears to reduce the average ripple voltage at their terminals. When a vehicle is unplugged, its battery is not charged. However, its terminal voltage is still being monitored by measurement blocks in the simulation. Hence, we see a smooth steady terminal voltage of about 406 V for the period t = 0.5 to 1.2 s in Figure 26.(v). The ripples reappear when charging is resumed in Vehicle 1, and decrease when Vehicle 2 is added to the charging profile.

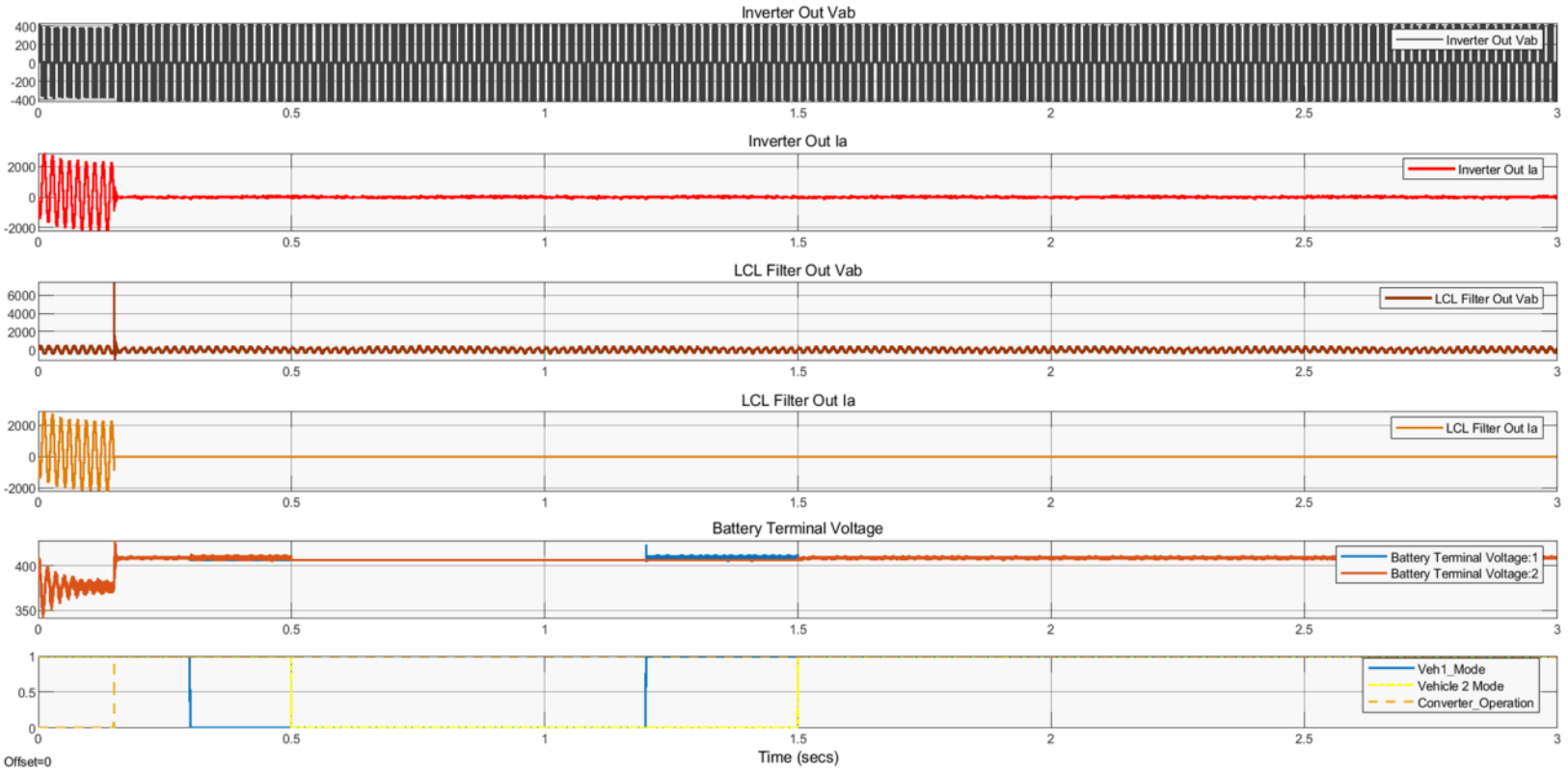

Figure 25. Plots, from time = 0 – 3 s, of inverter and LCL filter Phase A output voltages and currents, both vehicle battery terminal voltages and plug-in modes, and converter operating mode (1 = rectifier on & inverter off)

From top to bottom: (i) inverter Phase A output voltage, (ii) inverter Phase A output current, (iii) LCL filter Phase A output voltage, (iv) LCL filter Phase A output current, (v) Vehicles 1 & 2 battery terminal voltages on same axes, (vi) Vehicle 1 & 2 plug-in modes, and converter operating mode on same axes

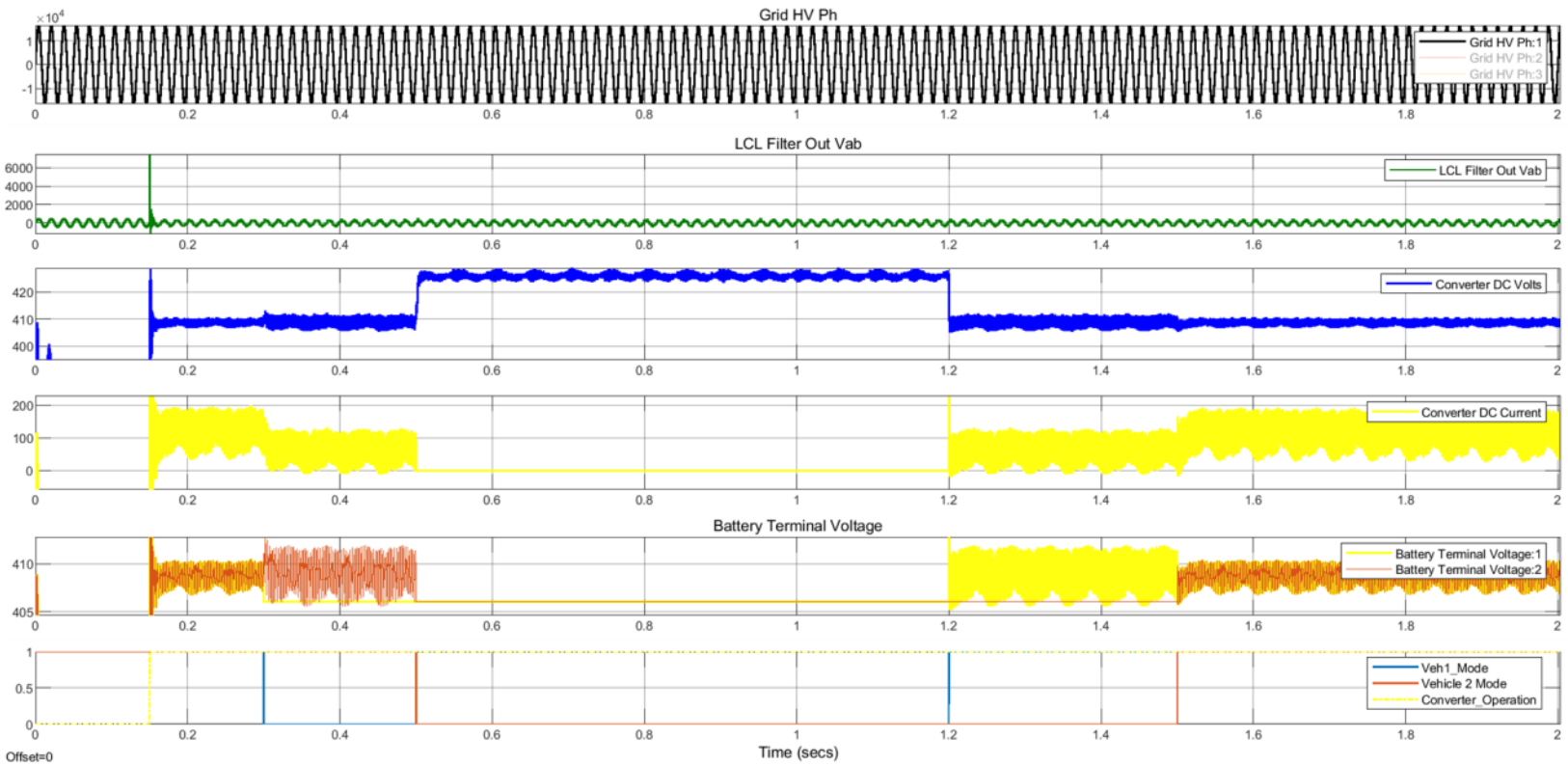

Figure 26. Plots, from time = 0 – 2 s, showing power grid phase voltage, LCL filter output voltage, and converter DC voltage and current, with varying vehicle charging loads in rectifier mode

From top to bottom: (i) Grid Phase A voltage, (ii) LCL filter Phase A output voltage, (iii) Converter DC voltage fed to batteries, (iv) converter DC current, (v) Vehicles 1 & 2 battery terminal voltages on same axes, (vi) Vehicles 1 & 2 plug-in modes, and converter operating mode on same axes

Figure 27 shows how the state of charge for each battery changes with time, increasing or decreasing depending on the V2G operational mode, but remaining flat when the corresponding vehicles are unplugged. The rectifier current increases with the number of vehicles being charged. However, its ripple current stays the same.

Figures 28 and 29 show expanded views of transients when mode transitions occur: first, immediately after the converter mode transitions from inverter to rectifier operation at 0.15 s, and later when the vehicles are unplugged (Vehicle 1 at 0.3 s and Vehicle 2 at 0.5 s) and plugged again (Vehicle 1 at 1.2 s and Vehicle 2 at 01.5 s). In Figure 28, which is an expansion of the plots from 't' = 0.1 s to 0.6 s, the charging current – shown in Figure 28.(ii) – settles to approximately 130 A at about 't'= 0.17 s, drops to about 65 A after Vehicle 1 is unplugged at 't' = 0.3 s, and drops further to 0 A after Vehicle 2 is also unplugged. There is a 360 Hz, 110 A peak-to-peak ripple in the current output of the rectifier. This frequency may be attributed to the switching operation of the six switches in the three-phase full-bridge rectifier operating on the 60 Hz grid voltage.

In Figure 29, which shows an expansion of the plots from 't' = 1.2 s to 1.6 s, the charging current – shown in Figure 29.(ii) – increases first to about 65 A when Vehicle 1 is plugged in, and further to about 130 A when the second vehicle is also plugged in. Gradual changes in the SoCs are also visible in the expanded plots in Figure 29.(iv).

It is also worth noting that though the rectifier exhibits significant ripple in its output current, the battery charging current at the output of the bi-directional AC-DC converter has significantly less ripple, due to the filtering effect of the DC link capacitor.

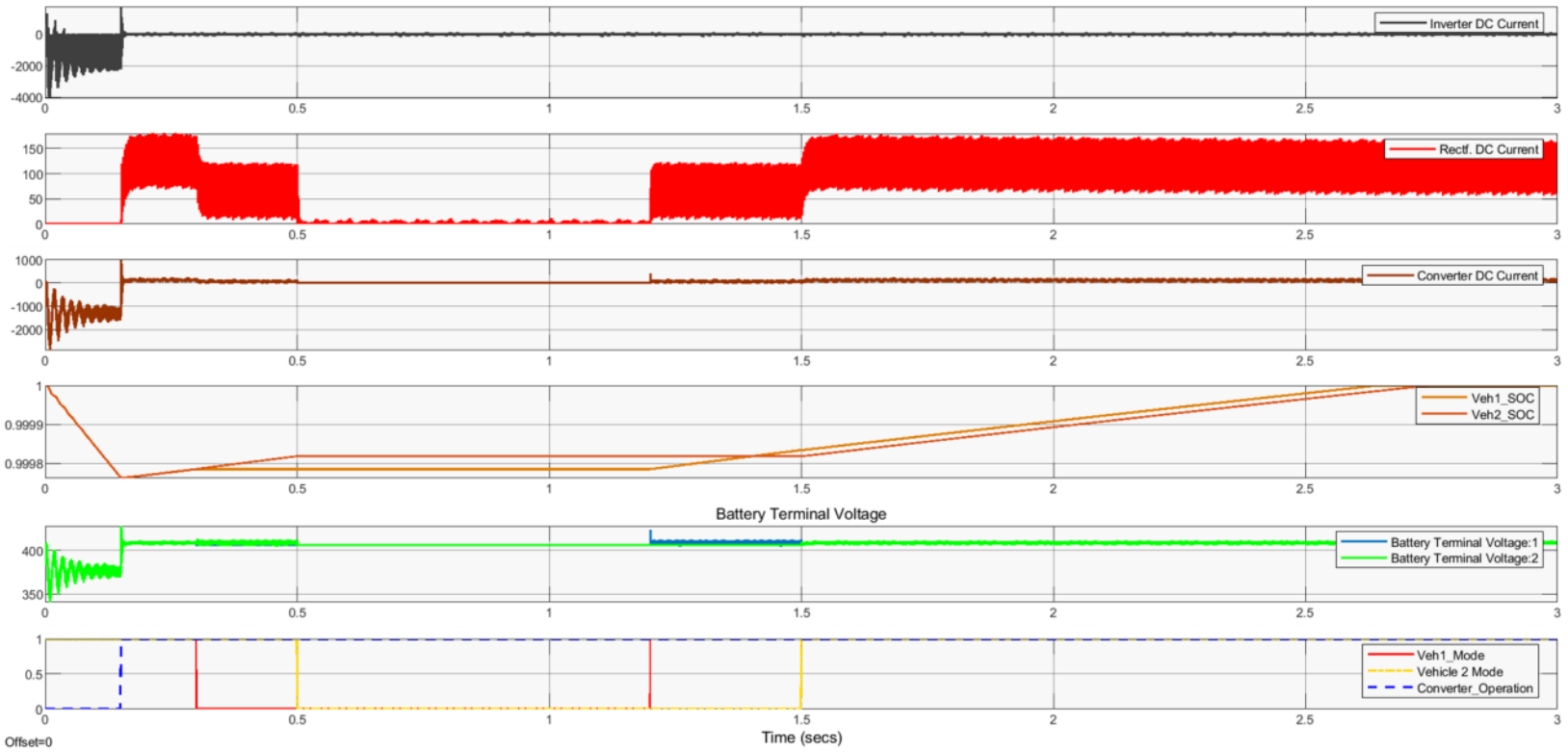

Figure 27. Plots, from time = 0 – 3 s, of rectifier DC output voltage and current, Vehicle 1 & 2 battery SoCs and plug-in states, battery terminal voltages, and converter operating mode (1 = rectifier on & inverter off)

From top to bottom: (i) inverter DC current, (ii) rectifier DC current, (iii) converter DC current, (iv) Vehicles 1 & 2 SoCs on same axes, (v) Vehicles 1 & 2 battery terminal voltages on same axes, (vi) Vehicle 1 & 2 plug-in modes, and converter operating mode on same axes

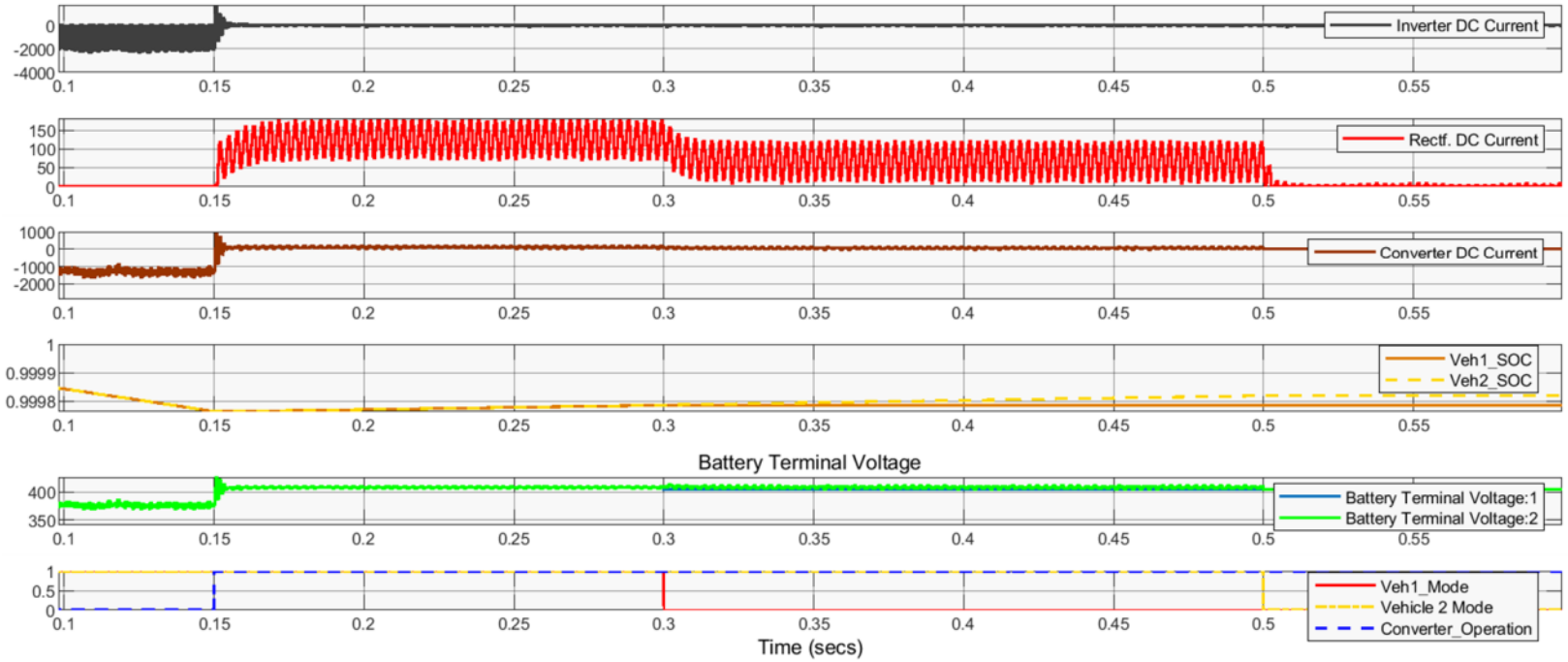

Figure 28. Expanded plots, from time = 0.1 – 0.6 s, showing converter voltage and current during vehicle charging load variations, Vehicle 1 & 2 battery SoCs and plug-in states, and converter operating mode

From top to bottom: (i) inverter DC current, (ii) rectifier DC current, (iii) converter DC current, (iv) Vehicles 1 & 2 SoCs on same axes, (v) Vehicles 1 & 2 battery terminal voltages on same axes, (vi) Vehicle 1 & 2 plug-in modes, and converter operating mode (1 = rectifier on, inverter off) on same axes

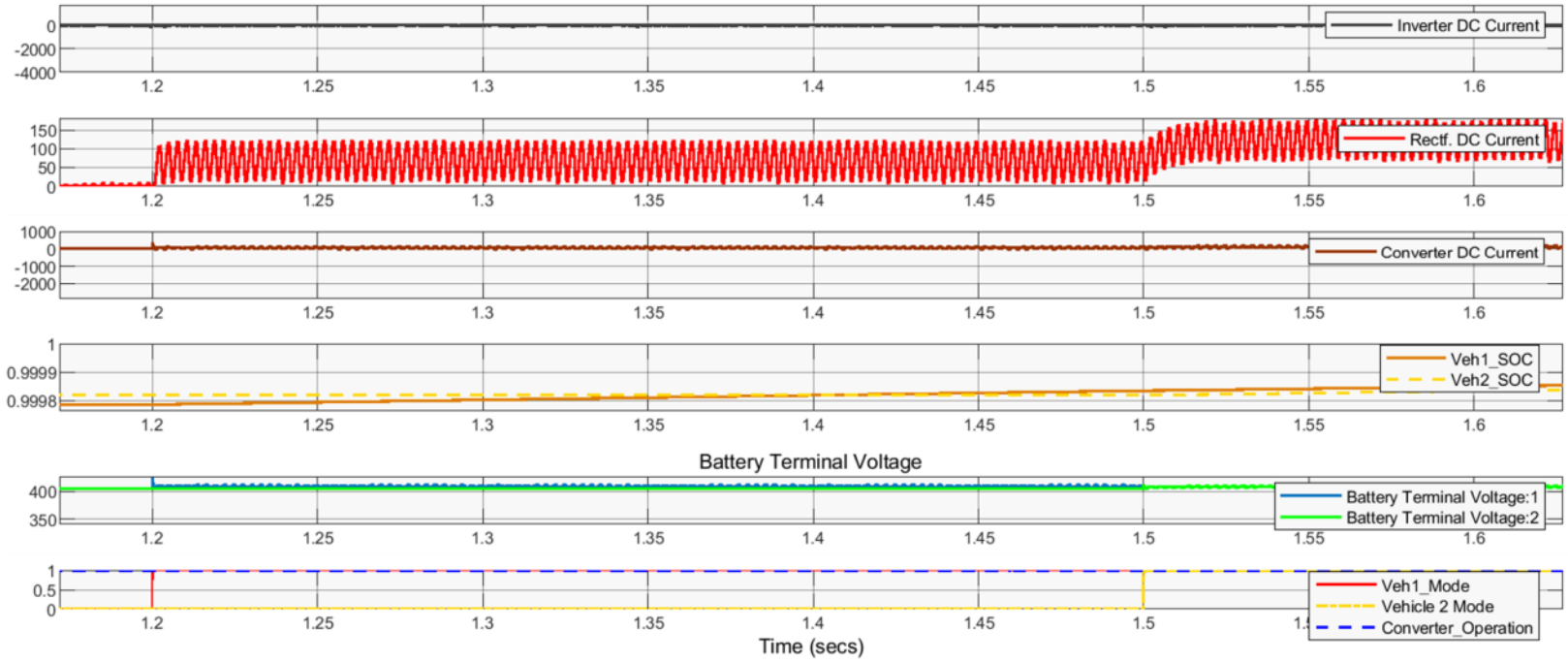

Figure 29. Expanded plots, from time = 1.2 – 1.6 s, showing converter voltage and current during charging load variations, Vehicle 1 & 2 battery SoCs and plug-in states, and converter operating mode

From top to bottom: (i) inverter DC current, (ii) rectifier DC current, (iii) converter DC current, (iv) Vehicles 1 & 2 SoCs on same axes, (v) Vehicles 1 & 2 battery terminal voltages on same axes, (vi) Vehicle 1 & 2 plug-in modes, and converter operating mode (1 = rectifier on, inverter off) on same axes

4.4. Results Summary

The tests confirm the stable operation of the V2G system in both grid injection and vehicle charging modes of operation. Furthermore, they reveal the effect of operating mode transitions and load variations on voltages and currents at different nodes, such as the vehicle battery terminals, the inverter output to the LCL filter and the AC-DC converter interfaces to both the power grid and vehicle fleet network.

In addition, the tests reveal characteristics of the transients at various system nodes. An interesting revelation is the presence of DC transients at the inverter output to the power grid, suggesting the need for some form of DC suppression at the output of the inverter to preserve power quality on the grid.

5. CONCLUSION

This study set out to model a V2G system with the functionality to examine transient interactions between a power grid and vehicle network. The model was also intended to support testing of control algorithms for practical V2G systems, including for example, the use of the vehicle network for smoothening of power flow on the grid.

The implemented V2G system model supports transient analysis under different operating conditions. In addition, it acts as a testbed capable of supporting future research into V2G systems. The design of the testbed incorporates numerous measurements at several points in the network topology. However, the focus has been on grid interactions and voltage and load fluctuations.

The tests performed in this study are not exhaustive; for example, the internal dynamics of individual batteries are not studied in-depth and SoCs are relied upon to measure the interaction between the batteries and the rest of the system. Using the readings and measurement points within the battery modules, there is the potential to discover additional useful information related to battery performance.

5.1. Thesis Contributions

A model of an AC-DC bi-directional converter subsystem has been constructed and tested for transient V2G studies. Duty-cycle models, in the form of vehicle plug-in profiles, have been built and incorporated within the model. The building blocks created are an extension to

existing functionality in Simulink® and will be useful for current and future research efforts that require a testbed for transient analysis of V2G systems.

5.2. Future Research Possibilities

Areas for further work and improvement include the incorporation of more sophisticated control modules to allow testing of complex grid management algorithms, including fuzzy-based schemes. Other possible future enhancements to the model include the inclusion of multiple converters in the model, options to scale up modules within the model to facilitate aggregate studies involving large V2G fleets, and the ability to have some vehicles operating in grid injection mode while others simultaneously operate in vehicle charging mode.

Additional enhancements include detailed specification of a transient model of a test feeder that can support V2G transient studies involving multi-node power grids. The model capabilities could also be extended to enable fault analyses in V2G systems.

Finally, given the current research interest in electric vehicle batteries, this model could prove useful in the testing of battery technologies once adequate battery models are built.

REFERENCES

[1] A. Briones, J. Francfort, P. Heitmann, M. Schey, S. Schey, and J. Smart, "Vehicle-to-Grid (V2G) Power Flow Regulations and Building Codes Review by the AVTA," Department of Energy (DOE), Idaho Falls, Rep. INL/EXT-12-26853, Sep. 2012. [Online]. Available: https://www.energy.gov/sites/prod/files/2014/02/f8/v2g_power_flow_rpt.pdf

[2] W. Kempton and J. Tomić, "Vehicle-to-grid power fundamentals: Calculating capacity and net revenue," *Journal of Power Sources*, vol. 144, no. 1, pp. 268-279, Jun. 2005. Accessed: Jan. 27, 2020. [Online]. Available: http://www.sciencedirect.com/science/article/pii/S0378775305000352, doi: 10.1016/j.jpowsour.2004.12.025.

[3] N. Zhou, J. Wang, Q. Wang and N. Wei, "Measurement-Based Harmonic Modeling of an Electric Vehicle Charging Station Using a Three-Phase Uncontrolled Rectifier," *IEEE Transactions on Smart Grid*, vol. 6, no. 3, pp. 1332-1340, May 2015. [Online]. Available: http://ieeexplore.ieee.org/stamp/stamp.jsp?tp=&arnumber=6983580&isnumber=7086423, doi: 10.1109/TSG.2014.2374675.

[4] Y. Ma, A. Cruden and D. Infield, "A Matlab simulator for electric drive vehicle to grid implementation," in *2010 IEEE International Conference on Industrial Technology*, Vina del Mar, Chile, 2010, pp. 1097-1101. [Online]. Available: https://www.researchgate.net/publication/251927163_A_Matlab_simulator_for_electric_drive_vehicle_to_grid_implementation, doi: 10.1109/ICIT.2010.5472577.

[5] T. A. Burress, S. L. Campbell, C. Coomer, C. W. Ayers, A. A. Wereszczak, J. P. Cunningham, L. D. Marlino, L. E. Seiber and H.-T. Lin, "Evaluation of the 2010 Toyota Prius Hybrid Synergy Drive System," U.S. Department of Energy, Washington, D.C., Rep. ORNL/TM-2010/253, Mar. 2011. [Online]. Available: https://info.ornl.gov/sites/publications/files/Pub26762.pdf, doi: 10.2172/1007833.

[6] D. Stephens, P. Shawcross, G. Stout, E. Sullivan, J. Saunders, S. Risser and J. Sayre, "HEV, PHEV, and BEV Battery System Analysis," in *Lithium-ion battery safety issues for electric and plug-in hybrid vehicles*, Washington, DC: National Highway Traffic Safety Administration, 2017, pp. 5-1. [Online]. Available: https://www.nhtsa.gov/sites/nhtsa.dot.gov/files/documents/12848-lithiumionsafetyhybrids_101217-v3-tag.pdf

[7] General Motors Co., "Chevrolet Pressroom: CHEVROLET VOLT - 2011," General Motors Co. Website, 2010. https://media.chevrolet.com/media/us/en/chevrolet/vehicles/volt/2011.html (accessed Nov. 13, 2020).

[8] U.S. Department of Energy, Office of Electricity Delivery and Energy Reliability, "United States Electricity Industry Primer," U.S. Department of Energy, Washington DC, 2015. [Online]. Available: https://www.energy.gov/sites/prod/files/2015/12/f28/united-states-electricity-industry-primer.pdf, doi: DOE/OE-0017.

[9] Eaton Corporation, plc., "Voltage regulators: fundamentals of power distribution voltage regulators," Eaton Corporation, plc. Website, 2020. https://www.eaton.com/us/en-us/products/medium-voltage-power-distribution-control-systems/voltage-regulators/voltage-regulators--fundamentals-of-voltage-regulators.html (accessed Nov. 8, 2020).

[10] J. Dong, Y. Xue, M. Olama, T. Kuruganti, J. Nutaro and C. Winstead, "Distribution Voltage Control: Current Status and Future Trends," in *2018 9th IEEE International Symposium on Power Electronics for Distributed Generation Systems (PEDG)*, Charlotte, NC, 2018, doi: 10.1109/PEDG.2018.8447628.

[11] S. Letendre, P. Denholm and P. Lilienthal, "Electric & Hybrid Cars: New Load, or New Resource?," *Public Utilities Fortnightly*, pp. 28-37, 2006. Accessed: Apr. 22, 2020. [Online]. Available: https://www.fortnightly.com/fortnightly/2006/12/electric-hybrid-cars-new-load-or-new-resource

[12] B. K. Sovacool, J. Axsen and W. Kempton, "The Future Promise of Vehicle-to-Grid (V2G) Integration: A Sociotechnical Review and Research Agenda," *Annual Review of Environment and Resources*, vol. 42, no. 1, pp. 377-406, 2017. [Online]. Available: https://doi.org/10.1146/annurev-environ-030117-020220, doi: 10.1146/annurev-environ-030117-020220.

[13] A. R. Bhatti, Z. Salam, M. J. B. A. Aziz, K. P. Yee and R. H. Ashique, "Electric vehicles charging using photovoltaic: Status and technological review," *Renewable and Sustainable Energy Reviews*, vol. 54, pp. 34-47, 2016. [Online]. Available: http://www.sciencedirect.com/science/article/pii/S1364032115010618, doi: 10.1016/j.rser.2015.09.091.

[14] M. Kerler, P. Burda, M. Baumann and M. Lienkamp, "A Concept of a High-Energy, Low-Voltage EV Battery Pack," in *2014 IEEE International Electric Vehicle Conference (IEVC)*, Florence, Italy, Dec. 2014. Accessed: Jul. 24, 2020. [Online]. Available: https://ieeexplore.ieee.org/document/7056185, doi: 10.1109/IEVC.2014.7056185.

[15] Tesla, Inc. and S. Nagaraj, "Application for TESLA, INC. 2019 model year test group KTSLV00.0L13 (Update)," Jan. 28, 2019. [Online]. Available: https://iaspub.epa.gov/otaqpub/display_file.jsp?docid=46584&flag=1 (accessed Nov. 8, 2020).

[16] A. Barai, T. Ashwin, C. Iraklis, A. McGordon and P. Jennings, "Scale-up of lithium-ion battery model parameters from cell level to module level – identification of current issues," *Energy Procedia*, vol. 138, pp. 223-228, 2017. [Online]. Available: http://www.sciencedirect.com/science/article/pii/S187661021735097X, doi: 10.1016/j.egypro.2017.10.154.

[17] T. Huria, M. Ceraolo, J. Gazzarri and R. Jackey, "High Fidelity Electrical Model with Thermal Dependence for Characterization and Simulation of High Power Lithium Battery Cells," in *2012 IEEE International Electric Vehicle Conference*, Greenville, SC, 2012, doi: 10.1109/IEVC.2012.6183271.

[18] M. H. Rashid, *Power Electronics: Devices, Circuits and Applications*, 4th ed., Upper Saddle River, New Jersey: Pearson Prentice Hall, 2014.

[19] C. C. Chan, "The State of the Art of Electric, Hybrid, and Fuel Cell Vehicles," *Proceedings of the IEEE*, vol. 95, no. 4, pp. 704-718, Apr. 2007, doi: 10.1109/JPROC.2007.892489.

[20] M. Aryanezhad, "Optimization of grid connected bidirectional V2G charger based on multi-objective algorithm," in *2017 8th Power Electronics, Drive Systems & Technologies Conference (PEDSTC)*, Mashhad, 2017, pp. 519-524, doi: 10.1109/PEDSTC.2017.7910381.

[21] M. Dursun and M. K. Döşoğlu, "LCL Filter Design for Grid Connected Three-Phase Inverter," in *2018 2nd International Symposium on Multidisciplinary Studies and Innovative Technologies (ISMSIT)*, Ankara, 2018, pp. 1-4. [Online]. Available: https://doi.org/10.1109/ISMSIT.2018.8567054, doi: 10.1109/ISMSIT.2018.8567054.

[22] B. K. Perera, P. Ciufo and S. Perera, "Point of common coupling (PCC) voltage control of a grid-connected solar photovoltaic (PV) system," in *IECON 2013 - 39th Annual Conference of the IEEE Industrial Electronics Society*, Vienna, 2013, pp. 7475-7480, doi: 10.1109/IECON.2013.6700377.

[23] B. Wu, H. Chen, G. Guan, T. Ding and L. Yin, "Simulation model of three-phase PWM rectifier charging station and harmonic analysis on grid," in *2017 IEEE Innovative Smart Grid Technologies - Asia (ISGT-Asia)*, Auckland, 2017, pp. 1-6, doi: 10.1109/ISGT-Asia.2017.8378340.

[24] W. H. Kersting, "Radial Distribution Test Feeders," *2001 IEEE Power Engineering Society Winter Meeting. Conference Proceedings (Cat. No.01CH37194)*, Columbus, OH, USA, vol. 2, Jan./Feb. 2001, pp. 908-912. Accessed: Jan. 29, 2020. [Online]. Available: https://site.ieee.org/pes-testfeeders/files/2017/08/testfeeders.pdf, doi: 10.1109/PESW.2001.916993.

[25] *IEEE PES Test Feeder Resources: 1992 Test Feeder Cases: 123-bus Feeder*," IEEE PES AMPS DSAS Test Feeder Working Group, Feb. 3, 2014. [Online]. Available: http://site.ieee.org/pes-testfeeders/files/2017/08/feeder123.zip, (accessed Jan. 29, 2020).

[26] The MathWorks, Inc., "MathWorks Help Documentation: Generic Battery Model - Simulink," The MathWorks, Inc. Website, 2020. https://www.mathworks.com/help/releases/R2019b/physmod/sps/powersys/ref/battery.html (accessed Aug. 12, 2020).

APPENDIX A

A. Simulink® Generic Battery and Modifications

Simulink® Generic Battery and Modifications

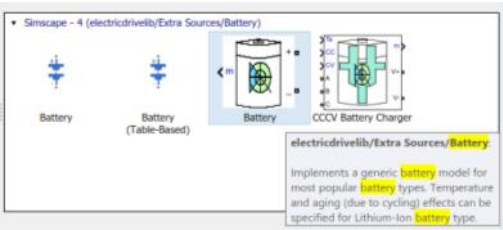

Generic battery model from Simulink [26]

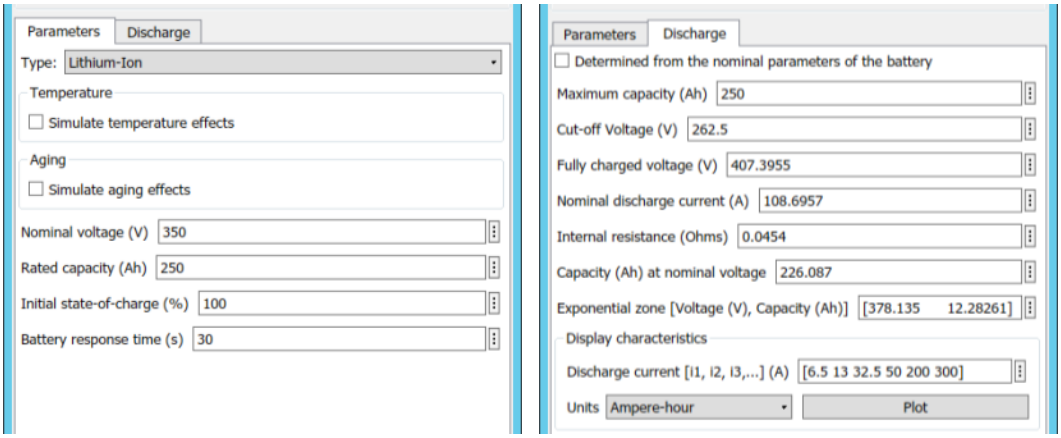

Modifications to generic battery model

APPENDIX B

B. Look-Up Table Data for the Li-Ion Battery SoC

Look-Up Table Data for the Li-Ion Battery SoC

Ah	V	SoC (calculated)
0	406.3	1
1.842	395.6	0.9926
1.965	395	0.9921
2.088	394.5	0.9916
3.071	390.7	0.9877
4.053	387.7	0.9838
6.018	383.5	0.9759
7.984	380.9	0.9681
9.949	379.3	0.9602
12.04	378.2	0.9518
13.57	377.7	0.9457
99.48	374.5	0.6020
149.2	371.6	0.4032
176.3	368.6	0.2948
199	364	0.204
208	361	0.168
212.5	359.1	0.15
217	356.7	0.132
219.3	355.3	0.1228
221.6	353.8	0.1136
223.8	352	0.1048
226.1	350	0.0956
229.8	346	0.0808
235	338.4	0.06
240.2	326.4	0.0392
242.7	317.5	0.0292
245.3	305.1	0.0188
250.5	256.4	-0.002
252.2	218.4	-0.0086